

Development of a CMAQ-PMF-based composite index for prescribing an effective ozone abatement strategy: A case study of sensitivity of surface ozone to precursor VOC species in southern Taiwan

5 Jackson Hian-Wui Chang^{1,2}, Stephen M. Griffith^{1#}, Steven Soon-Kai Kong¹, Ming-Tung Chuang³, Neng-Huei Lin^{1,4,*}

¹Department of Atmospheric Sciences, National Central University, Taoyuan, 32001, Taiwan

²Preparatory Center for Science and Technology, University Malaysia Sabah, Jalan UMS, 88400, Kota Kinabalu, Sabah, Malaysia

10 ³Research Center for Environmental Changes, Academia Sinica, Taipei 11529, Taiwan

⁴Center for Environmental Monitoring and Technology, National Central University, Taoyuan, 32001, Taiwan

[#]Presently affiliated with Department of Atmospheric Sciences, National Taiwan University, Taipei 10617, Taiwan

Correspondence to: Neng-Huei Lin (nhlin@cc.ncu.edu.tw)

15 **Abstract.** Photochemical ozone pollution is a serious air quality problem under weak synoptic conditions in many areas worldwide. Volatile organic compounds (VOCs) are largely responsible for ozone production in urban areas where NO_x mixing ratios are high while usually not a limiting precursor to ozone. In this study, the Community Multiscale Air Quality model – Higher-order Direct Decoupled Method (CMAQ-HDDM) at an urban-scale resolution (1.0 km x 1.0 km) in conjunction with positive matrix factorization (PMF) was used to identify the dominant sources of highly sensitive VOC
20 species to ozone formation in southern Taiwan, a complex region of coastal urban and industrial parks and inland mountainous areas. First-order, second-order and cross sensitivities of ozone concentrations to domain-wide (i.e. urban, suburban and rural) NO_x and VOC emissions were determined for the study area. Negative (positive) first-order sensitivities to NO_x emissions are dominant over urban (inland) areas, confirming ozone production sensitivity favors the VOC-limited regime (NO_x-limited regime) in southern Taiwan. Furthermore, most of the urban areas also exhibited negative second-order
25 sensitivity to NO_x emissions, indicating a negative O₃ convex response where the linear increase of O₃ from decreasing NO_x emissions was largely attenuated by the non-linear effects. Due to the solidly VOC-limited regime and the relative insensitivity of O₃ production to increases or decreases of NO_x emissions, this study pursued the VOC species that contributed the most to ozone formation. PMF analysis driven by VOCs resolved 8 factors including mixed industry (21%),

vehicle emissions (22%), solvent usage (17%), biogenic (12%), plastic industry (10%), aged air mass (7%), motorcycle
30 exhausts (7%), and manufacturing industry (5%). Furthermore, a composite index that quantitatively combined the CMAQ-
HDDM sensitivity coefficient and PMF resolved factor contribution, was developed to identify the key VOC species that
should be targeted for effective ozone abatement. Our results indicate that VOC control measures should target on (1)
solvent usage for painting, coating and the printing industry, which emits abundant toluene and xylene, (2) gasoline fuel
vehicle emissions of n-butane, isopentane, isobutane and n-pentane, and (3) ethylene and propylene emissions from the
35 petrochemical industry.

1. Introduction

Photochemical production of tropospheric ozone (O_3) depends in a nonlinear manner on the availability of nitrogen oxides
(NO_x) and volatile organic compounds (VOCs). Understanding ozone formation sensitivity to NO_x and VOC emissions is
40 key to developing effective abatement strategies on O_3 pollution in heavily-polluted cities. Brute-force method (BFM) has
often been used to address the relationship between O_3 and its precursors (Hakami et al., 2004; Li et al., 2013; Zhang et al.,
2009). In a BFM approach within a 3D-modeling framework (e.g. Community Multiscale Air Quality modeling system –
CMAQ), individual emissions are perturbed by a small amount and the model response is recorded against the baseline,
representing the sensitivity coefficient. However, the linear response of BFM is insufficient to account for changes in
45 secondary pollutants (i.e. ozone) generated by nonlinear interactions of various substances. Therefore, more sophisticated
numerical techniques have been introduced such as the adjoint method (Hakami et al., 2006; Wang et al., 2021), Decoupled
Direct Method in Three Dimensions – DDM 3D (Dunker et al., 2002b; Luecken et al., 2018), and higher-order decoupled
direct method – HDDM 3D (Cohan et al., 2005; Koplitz et al., 2021), where the 3D aspect is specific to implementation in
chemical transport models (CTMs) with a 3D-modeling framework (e.g. CMAQ). These methods offer an alternative to
50 BFM by directly solving the auxiliary equations that represent the change in concentration over change in emission (dC/dE)
derived from the governing equations of the model.

DDM 3D, using a semi-implicit finite difference scheme with different time steps (Hakami et al., 2004; Yang et al., 1997),
has been widely implemented in CTMs (Dunker et al., 2002b, 2002a) to calculate the first-order sensitivities (i.e. tangential,

55 $\partial C/\partial E$) of ozone with respect to initial concentration, boundary concentrations, and precursor emission rates. First-order sensitivity describes the linear response of the model to a perturbed input parameter, while higher-order sensitivity describes the nonlinear quadratic, cubic and higher-power responses. In the presence of strong nonlinearity (e.g. in transition between VOC-limited and NO_x-limited regime), first-order sensitivity alone may be insufficient to characterize the response if the magnitude of the emissions changes are large (i.e. a manifestation of the nonlinear chemistry involved in ozone formation)
60 and second-order sensitivity is necessary to provide the additional nonlinear responses of the system (Xing et al., 2011; Xiao et al., 2010). Thus, in HDDM, the sensitivity is calculated by solving the first-order ($\partial C/\partial E$) and second-order (i.e. local slope, $\partial^2 C/\partial E^2$) derivatives in the model when a relative perturbation (e.g. $\pm 10\%$) is applied to a targeted parameter while keeping all other factors constant.

65 Apportioning pollutant concentrations to their sources is an ideal strategy to guide emission control policy (Dunker et al., 2015; Liu et al., 2008). However, source apportionment of a secondary pollutant such as ozone is complex, where a relatively crude method is to simply conduct simulations with and without NO_x and VOC emissions from a given source so that the difference in ozone concentration is a measure of the source contribution (Bergin et al., 2008). Other source apportionment approaches such as ozone source apportionment technology (OSAT) and integrated source apportionment
70 method (ISAM) are embedded into air quality models (Comprehensive Air Quality Model with Extensions (CAMx) and CMAQ, respectively) and rely on tagging NO_x and VOCs as tracers from emission to ozone production to estimate the contributions of different sources to the eventual ozone concentration (Dunker et al., 2002a; Kwok et al., 2015). Unless a high resolution sector profile emission inventory is available, the application of OSAT and ISAM is often limited to four main sector groups: on-road, non-point (area), point, and biogenic sources (Wang et al., 2009; Li et al., 2013a). In addition,
75 the spatio-temporal and sector group distribution uncertainties associated with the emission inventory greatly influence the accuracy of these source apportionment methods (Zheng et al., 2009).

Positive matrix factorization (PMF), a receptor-based approach, offers an alternative to those embedded methods by generating a set of ozone precursor source composition profiles, each identifying a mix of compounds associated with a

80 particular category of emissions. Driven by measured concentrations at receptor sites, PMF can be used as an ozone source apportionment method directly and is independent of the uncertainties associated with the emission inventory. In recent years, PMF has been widely used to estimate VOC apportionment because it requires only identifying characteristics of the source profiles to interpret the PMF factors (Ji et al., 2022; Fan et al., 2021; Huang and Hsieh, 2020; Chen et al., 2019; Wu et al., 2016). For instance, Pallavi et al. (2019) found that traffic contributed 47% of the total benzene in India followed by
85 residential biofuel use and waste disposal (25%) and industrial emissions and solvent use (20%). Zhao et al. (2020) used PMF in conjunction with an ozone formation potential (OFP) calculation to infer that VOCs from industrial and vehicular emissions were the dominant ozone precursors in Nanjing, East China, particularly xylenes, toluene, and propene. Chen et al. (2019) used PMF to resolve the dominant VOC sources at an industrial complex in central Taiwan and found that the monitored VOC concentrations of vehicle exhaust, solvent use, and diesel attributed to high OFP were associated with
90 easterly to southeasterly winds. Huang and Hsieh (2020) analyzed VOC data by PMF from western coastal Taiwan and suggested that on a mass concentration basis industrial emissions are the greatest contributors to OFP. However, previous PMF-OFP studies have only identified key VOC sources to OFP without investigating the sensitivity of OFP to these VOC emissions and thus failed to provide comprehensive advice on which sources to prioritize for effective ozone abatement.

95 In this work, we used CMAQ-HDDM-3D in conjunction with PMF, enabling us to interpret the sensitivity and source apportionment analyses together for a more comprehensive investigation of the key VOC sources to OFP. We combined the two approaches as a novel methodology to provide additional insights on the dominant sources of highly sensitive VOC species to ozone formation in a VOC-limited urban area of Taiwan, but should be widely applicable across urban areas that experience similar O₃ episodes such as Hong Kong (Ling and Guo, 2014), Beijing and Hebei (Chi et al., 2018), Mexico City
100 (Lei et al., 2007), Houston, United States (Mazzuca et al., 2016). Specifically, HDDM describes the O₃ sensitivity response to a speciated emission and PMF identified the sources of these species for effective ozone abatement strategy. While most of the HDDM sensitivity studies are performed at coarse resolution (>4.0 km), this study was conducted at urban-scale resolution (1.0 km x 1.0 km). We investigated the first-order, second-order, and cross sensitivities of ozone concentrations to domain-wide NO_x and VOC emissions and provide an overview of the O₃-precursors sensitivity across the study area. We

105 then identified the VOC species to which ozone formation was most sensitive. Finally, we mapped these highly sensitive
VOC species to the PMF model source apportionment and identified their dominant sources for effective emission control
strategies using a composite index of CMAQ sensitivities and PMF factor contributions. The results of our study provide
important information as to which VOC species are key to ozone formation and where to reduce sources of these VOC
species for effective ozone abatement.

110

2. Methods

2.1 Study Period & Area

In this study, we selected the period from 07-20 Oct. 2018 for conducting simulations of photochemical ozone production
and transport in southern Taiwan. The selected case in October 2018 is the seasonal transition period when the summer
115 season is in transition to the winter. The case can reasonably represent the typical ozone pollution conditions during seasonal
transition period in Taiwan because the synoptic weather pattern of the event features a weak intrusion of Asian continental
anticyclone system which slowly propagated eastward causing the prevailing wind in Taiwan dominated by weak
northeasterly (NE) flows due to continental high-pressure peripheral circulation (see Figure S1). Hsu & Cheng (2019)
identified six synoptic weather patterns common in Taiwan and studied the characteristics of corresponding air pollutants in
120 each pattern using 6 years (2013-2018) daily averaged wind fields and sea-level pressure observed at surface weather
stations in Taiwan. Among the six patterns (C1-C6), C4 has the highest mean O₃ concentrations and occurs predominantly in
October. It features a weak anticyclone over the Asian continent and the Pacific subtropical high-pressure system does not
have an apparent influence in Taiwan, which is similar to our selected case in October 2018. Although the photochemistry is
strong in summer season, the seasonal O₃ variation in Taiwan shows that the monthly O₃ concentration is relatively higher
125 during the seasonal transition months (i.e., October) compared to other seasons (Hsu and Cheng, 2019; Chen et al., 2021;
Cheng et al., 2015). This is because during the seasonal transition months, when the photochemical reaction is still strong
compared to that of the winter months together with the reduced ventilation capability, the O₃ concentration can accumulate
(Yen and Chen, 2000; Tsai et al., 2008) (See Figure S2 for ozone seasonality in Taiwan). During the seasonal transition
period in autumn, southern Taiwan often suffers from high O₃ episodes (Hsu and Cheng, 2019; Chen et al., 2004, 2021).

130 Regional synoptic weather in autumn usually features a weak anticyclone over the Asian continent, allowing for local accumulation of pollutants, while the Pacific subtropical high-pressure system has shifted eastward with no apparent influence on Taiwan (Hsu and Cheng, 2019). This synoptic weather pattern is also categorized as High Pressure Pushing (HPP), which occurred when the leading edge of Asian continental high-pressure systems moves over China coastal provinces and carried pollutants southward towards downwind area in Taiwan (Chuang et al., 2008). In addition, 135 precipitation is less and vertical dispersion is weaker than in summer (Yen and Chen, 2000; Tsai et al., 2008), which contribute to relatively more frequent ozone episodes in autumn. These conditions are also common occurrences for high O₃ episodes in other places such as Hong Kong and East China cities in autumn (Lee et al., 2009; Liu et al., 2021; Yu et al., 2021). A 5-day spin-up period (02-06 Oct. 2018) was discarded from the analysis to eliminate the effects of initial conditions on O₃ simulations.

140

Since the 1990s, ozone concentrations have been increasing in many areas of southern Taiwan (Chang et al., 2005; Chen et al., 2021). Kaohsiung city, the biggest city in southern Taiwan and second biggest in all of Taiwan, hosts many heavy industries, including petrochemical plants, refineries, steel-making plants, and power generation plants. Xiaogang (XG) district is located in the southeastern portion of the city and hosts a petrochemical industrial park with an overall area of 403 145 hectares. Three power plants, each producing 1200-4300 MW day⁻¹, are located within a distance of 35 km of XG, and lead to some of the poorest air quality in Taiwan.

2.2 WRF-CMAQ Model Configuration

WRF model version 3.9.1 and CMAQ model version 5.2.1 (WRF-CMAQ) is used in the current study with a domain 150 configuration of a four-nested grid system centered at 28°N and 125°W (Figure 1a). The outermost domain (D01) covers most of mainland China with a horizontal resolution 27 km x 27 km and 166 x 169 grids, which is then nested to the second domain (D02) of 9 km x 9 km and 223 x 223 grids over East China. The third domain (D03) covers the whole island of Taiwan with a resolution of 3 km x 3 km and 223 x 223 grids and the innermost domain (D04) focuses on southern Taiwan

with a 1 km x 1 km resolution and 136 x 136 grids. There are 41 vertical sigma layers spaced unequally from the ground to
155 the model top 50 hPa, with the bottom 8 layers resolved below 1.5 km (Figure S3).

The initial and boundary meteorological conditions are adopted from the National Centers for Environmental Prediction
(NCEP) global final analysis (FNL) data at 0.25° x 0.25° resolution updated every 6 hours. The projected 2017-year Multi-
resolution Emission Inventory for China (available at <http://meicmodel.org>) with 0.25° x 0.25° resolution is used for D01
160 and D02, while 2016 Taiwan Emission Data System (TEDS) version 10 (Figure 1(c, d)) is used for D03 and D04. Biogenic
emissions are calculated offline using Model of Emissions of Gases and Aerosols from Nature (MEGAN) version 2.10
(Guenther et al., 2006).

Other than local anthropogenic emissions, the contribution of long-range transport (LRT) from East Asia (e.g. Chinese
165 emissions) is also substantial to Taiwan's air quality especially under strong northeasterly winds condition (Wu and Huang,
2021; Chang et al., 2022a). Lin et al. (2004) identified three types of common LRT events in Taiwan: (1) dust storm (DS),
LRT with pollutants (frontal pollution; FP), and (3) LRT of background airmasses (BG). When there is no frontal system,
local pollution (LP) dominates the air quality in Taiwan. During wintertime and springtime, the occurrence of LP cases were
70% and about 30% were LRT cases (Lin et al., 2004). Lin et al. (2005) estimated that the long-range transport of pollutants
170 contributes to about 30 $\mu\text{g m}^{-3}$, 230 ppb and 0.5 ppb to the PM_{10} , CO, and SO_2 concentrations, respectively, in northern and
eastern Taiwan. Meanwhile a smaller contribution is estimated in southern Taiwan due to the geographic (Lin et al., 2005).

In our work, the oceanic chlorine emission is calculated online by CMAQ as a function of meteorology using an OCEAN
file which specifies the fraction of each grid cell that is open ocean (OPEN) or surf zone (SURF). Figure 2a-c presents the
175 spatial distribution of CMAQ calculated sea-salt aerosol cations (ASEACAT - Na^+ , K^+ , Ca^{2+} and Mg^{2+}), fine-mode chlorine
and coarse-mode chlorine emission rates averaged during the entire simulation period. The sea-spray emissions were higher
in the surf zone area and highest emission rates were found along the eastern offshore of southern Taiwan. This is because of
the enhanced formation of sea-spray aerosols associated with higher relative humidity and greater offshore winds along the

eastern offshore of southern Taiwan that is open to the Western Pacific Ocean. Besides, the anthropogenic chlorine emissions (PCL) are obtained from TEDS v10 emissions, and they are concentrated over the heavily industrialized urban areas of southern Taiwan (see Figure 2d).

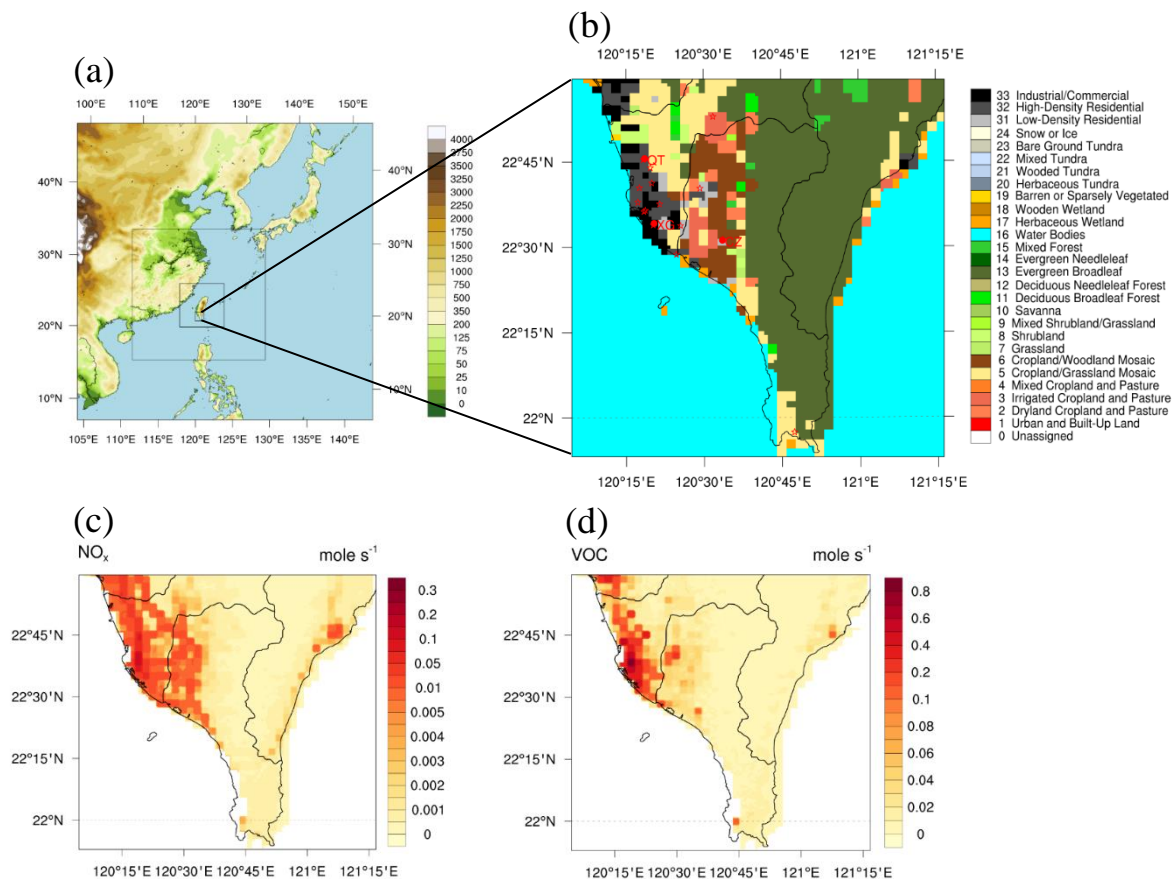


Figure 1: (a) Domain configuration of four-nested grid system, (b) land use of the innermost domain; “urban” and “inland” areas are represented by Class 31, 32, 33 and Class 6, respectively, (c,d) monthly averaged NO_x and VOC emissions in the innermost domain obtained from 2016 TEDS-10 emission inventory. The location of each TEPA air quality stations (red stars) and PAMS stations (red dots with label) used in the current study are displayed in the innermost domain. Refer Figure S3 and Table S3 for details of each TEPA and PAMS station.

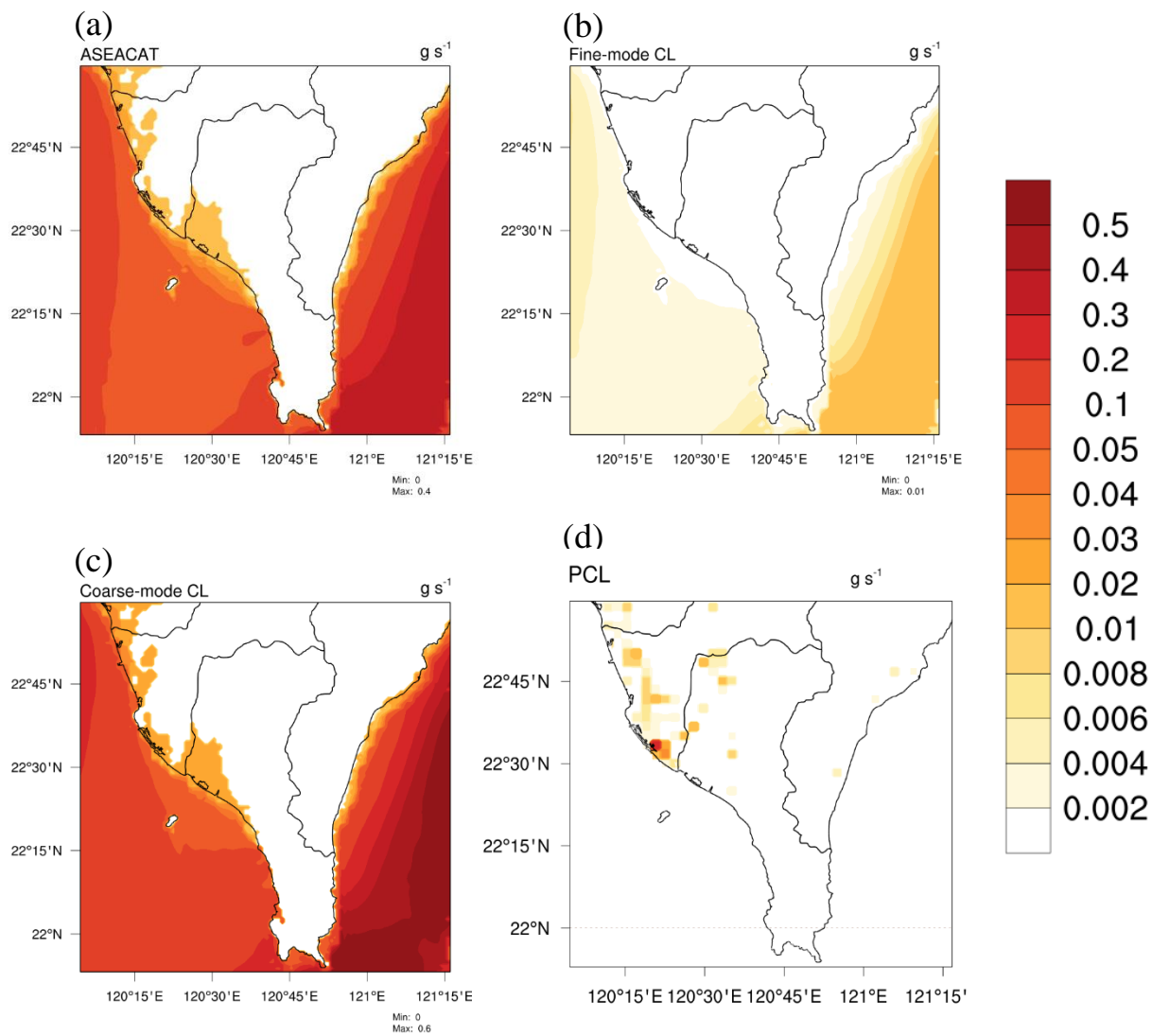


Figure 2: CMAQ calculated (a) sea-salt aerosol cations (ASEACAT) emissions (Na^+ , K^+ , Ca^{2+} and Mg^{2+}), (b) fine-mode chlorine SSA emissions, (c) coarse-mode chlorine SSA emissions and (d) TEDS v10 anthropogenic chlorine (PCL) emissions averaged during the entire simulation period.

To obtain more accurate dynamical downscaling, grid nudging was applied in the coarse domain D01 and D02; observation nudging was applied in the fine domain D03 and D04. Grid nudging is applied to the horizontal wind components, potential temperature, and water vapor mixing ratio; it is only applied above the PBL. The observational data for observation nudging include hourly surface observations such as atmospheric pressure, air temperature, relative humidity, wind speed and wind direction from 36 surface meteorological stations (<https://www.epa.gov.tw/>), and the twice-daily at 00:00 and 12:00 UTC sounding data such as potential height, temperature, dew point temperature, RH, wind direction, wind speed at each specified isobaric level from 2 radiosonde observation stations in Taiwan. The nudging coefficients, which determine the strength of the assimilation tendency term were set to be 6×10^{-4} for observation nudging and 3×10^{-4} for grid nudging. These values of coefficients were recommended by the WRF user guide and tested to be appropriate in previous studies (Li et al., 2022; Borge et al., 2008).

The simulation adopted the Carbon-Bond Mechanism CB6 (Yarwood et al., 2010), which was developed as an update to CB05 to provide a condensed chemical mechanism for use in atmospheric models. CB6 includes five additional organic compounds that are long-lived and relatively abundant (i.e. propane, acetone, benzene, ethyne, and higher ketones) and a more detailed representation of organic nitrate reactions. CB6 has been tested against measurements over a wide variety of spatial, temporal, chemical and meteorological conditions and has shown good agreement with measurements of ozone and nitrogen oxides in both urban and rural areas (Luecken et al., 2019). The halogen chemistry in CB6 considers chlorine-related reactions such as ClNO_2 , HCl and HNO_3 production from heterogeneous uptake of N_2O_5 on the aerosol surface, which are important to ozone pollution over coastal cities in southern Taiwan.

The Noah land surface model (LSM) is used to describe the land-atmosphere interaction (Chen and Dudhia, 2001). The urban effect in Noah LSM is invoked by implementing a single-layer urban canopy model (UCM), which assumes infinitely long 2D street canyon urban geometry to improve the processes associated with the exchange of momentum, heat, and moisture in the urban environment (Kusaka and Kimura, 2004; Kusaka et al., 2001). To take full advantage of the UCM

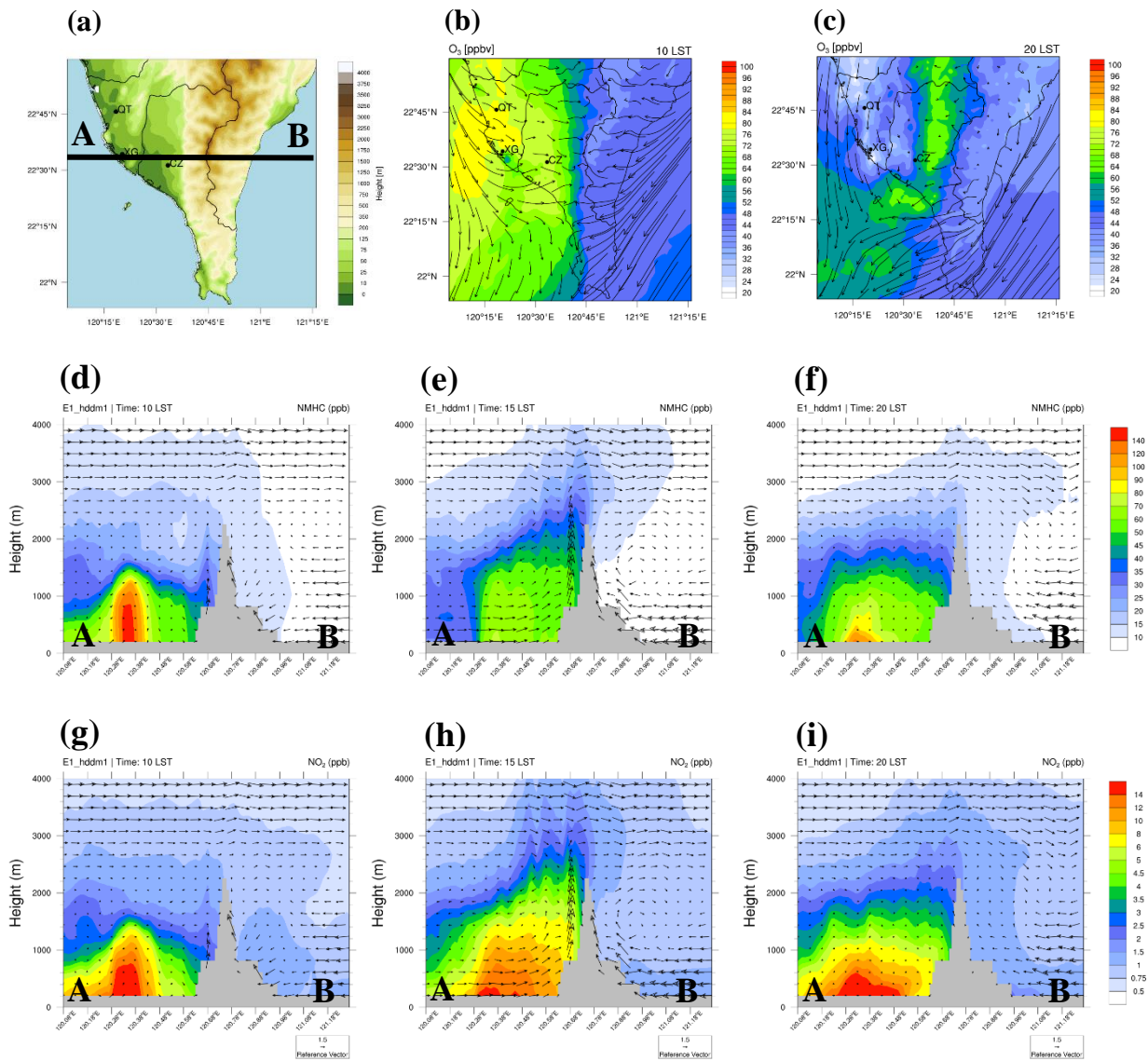
scheme, three additional urban classes (i.e. low-density residential, high-density residential and industrial/commercial) are further classified for better representation of the urban features (Figure 1b).

225 The asymmetric convective model version 2 (ACM2) boundary layer scheme is selected to represent the boundary layer process (Pleim, 2007). It includes the nonlocal scheme of the original ACM combined with an eddy diffusion scheme. Thus, ACM2 is able to represent both the supergrid- and subgrid-scale components of turbulent transport in the convective boundary layer. Also used were the Goddard Cumulus Ensemble (GCE) microphysics scheme (Tao et al., 2003), Radiative Transfer Model (RRTM) longwave radiation scheme (Gallus and Bresch, 2006), Goddard shortwave radiation scheme (Chou and Suarez, 1999), Monin-Obukhov similarity scheme, and Kain-Fritsch cumulus parameterization scheme (only at D01 and
230 D02).

The modeled results of both meteorology (i.e. 2m-temperature, wind speed & direction and relative humidity) and air quality (i.e. ozone, nitrogen oxides and volatile organic compounds) are validated against 15 Taiwan Environmental Protection Administration (TEPA) air quality stations. Overall, the modeling system reproduced the observed meteorological and air
235 quality conditions within the benchmark values (see Supplementary Material – Model Evaluations).

The “urban” and “inland” grid cells are defined according to the USGS-24 Land Use Category. “Urban” area is represented by Class 1 - Urban and Built-up Land, which we further classified into Class 31, 32, 33 (see Figure 1b) for WRF Single-Layer Urban Canopy Scheme (SLUCM) simulation. We refer the readers to our previous work for detailed discussion on the
240 land use classification and SLUCM implementation in (Chang et al., 2022b). “Inland” area is represented by Class 6 – Cropland/Woodland Mosaic (see Figure 1b). The general meteorological pattern of the event features a weak intrusion of Asian continental anticyclone system which slowly propagated eastward causing the prevailing wind at synoptic scale in Taiwan dominated by weak northeasterly (NE) flows due to continental high-pressure peripheral circulation (see Figure S1). At local scale in southern Taiwan, the steering of weak NE flows by the orographic effect of the Central Mountain Range

245 (CMR) enhanced the local circulations (i.e. land-sea breeze), and eventually pushed the locally produced urban O_3 as well as its precursors NO_x and NMHC towards the inland areas (see Figure 3).



250 Figure 3: (a) Topography of the innermost domain. (b, c) Spatial distribution of O_3 concentration averaged during the entire simulation at 10 LST and 20 LST, respectively. (d-f) Vertical profile of NMHC concentration cross sectioned at AB (see

Figure 3a) averaged during the entire simulation at 10 LST, 15 LST, and 20 LST, respectively. (h-i) Same as d-f but for NO₂ concentration.

2.3 Higher-order Decoupled Direct Method (HDDM)

255 The response of a chemical concentration to perturbations in model parameters (i.e. emissions, initial condition, boundary condition and reaction rate constants) can be evaluated through sensitivity analysis. A perturbed sensitivity parameter, p_i , is related to the unperturbed sensitivity parameter, P_i , in the baseline simulation as:

$$p_i = \varepsilon_i P_i = (1 + \Delta\varepsilon_i) P_i \quad (1)$$

where ε_i is a scaling factor with a nominal value of 1.0 when there is no perturbation, and $\Delta\varepsilon_i$ is a perturbed scaling factor.

260 The response of a chemical concentration, C , against the perturbations in a sensitivity parameter, p_i , is defined as the sensitivity coefficient, S_i . The first- and second-order sensitivity coefficients, $S_i(1)$, and $S_{i,j}(2)$ are defined as follows:

$$S_i^{(1)} = P_i \frac{\partial C}{\partial p_i} = P_i \frac{\partial C}{\partial(\varepsilon_i P_i)} = \frac{\partial C}{\partial \varepsilon_i} \quad (2)$$

$$S_{i,j}^{(2)} = P_i \frac{\partial C}{\partial p_i} P_j \frac{\partial C}{\partial p_j} = P_i \frac{\partial C}{\partial(\varepsilon_i P_i)} P_j \frac{\partial C}{\partial(\varepsilon_j P_j)} = \frac{\partial^2 C}{\partial \varepsilon_i \partial \varepsilon_j} \quad (3)$$

Both $S_i(1)$, and $S_{i,j}(2)$ have the same units as the chemical concentration, C . $S_i(1)$ measures the impact of one variable p_i on a
 265 concentration, C ; $S_{i,j}(2)$ measures the impact of another variable p_j on a first-order sensitivity, $S_i(1)$, which can be used to investigate the second-order cross sensitivity of the system. When $i=j$, $S_{i,i}(2)$ represents the local curvature of the relationship between a concentration and a single parameter, thus indicating the responsiveness of C to a broad range of p_i and describing a nonlinearity of the system. A second-order sensitivity of zero indicates a perfectly linear response, while greater values represent proportionally greater non-linearity effects. Matching signs of the sensitivities (e.g. positive first-order and positive
 270 second-order) represent a convex response while opposite signs represent a concave response (Figure S4). In the context of our study, reduced emission is the focus so a convex response represents a non-linear ozone concentration decrease with decreasing emissions and a concave response represents a non-linear ozone concentration increase with decreasing emissions.

275 **2.3.1 Taylor Series Expansion**

After determining the sensitivity coefficients, we can apply these coefficients for estimating the concentration changes in emission reduction scenarios based on Taylor series expansion. The concentration change from any fractional perturbations in a sensitivity parameter are approximated by (Cohan et al., 2005):

$$C_i |_{p_i=P_i+\Delta\varepsilon_i P_i} \approx C_o |_{p_i=P_i} + \Delta\varepsilon_i S_i^{(1)} + \frac{1}{2} \Delta\varepsilon_i^2 S_{i,i}^{(2)} + \dots + \frac{1}{n} \Delta\varepsilon_i^n S^{(n)} \quad (4)$$

280 where C_i is the concentration when p_i has been perturbed by an amount $\Delta\varepsilon_i P_i$. Subscript i represents the targeted emission species (i.e. a NO_x or VOC species). When multiple sensitivity parameters are perturbed simultaneously, a second-order Taylor approximation includes the interaction between the two parameters (Cohan et al., 2005):

$$C_{i+j} \cong C |_{p_{i,j}=P_{i,j}+\Delta\varepsilon_{i,j} P_{i,j}} \approx C_o + \Delta\varepsilon_i S_i^{(1)} + \Delta\varepsilon_j S_j^{(1)} + \frac{1}{2} \Delta\varepsilon_i^2 S_{i,i}^{(2)} + \frac{1}{2} \Delta\varepsilon_j^2 S_{j,j}^{(2)} + \Delta\varepsilon_i \Delta\varepsilon_j S_{i,j}^{(2)} + \dots \quad (5)$$

where $S_{i,j}$ is the cross sensitivity between the two parameters, which differs from the sum of the two sensitivities, S_i and S_j .

285

In this study, CMAQ-HDDM-3D [v5.2.1](#) is used to calculate the sensitivity coefficients to predict the O₃ response to perturbations in NO_x and VOC emissions. Perturbations at $\pm 10\%$ were made on the domain-wide emissions of NO_x and VOCs (D01-D04) from both anthropogenic and biogenic sources, but only sensitivity coefficients from the innermost domain (D04) are used for data analysis. A total of 25 sensitivity tests were performed to quantify the change in O₃ concentration due to the perturbations made in each test (Table 1); the first 5 sensitivity tests, S1-S5, account for the first-order, second-order and cross sensitivity due to the perturbed NO_x and total VOC emissions and the other 20 sensitivity tests, S6-S25, account for sensitivities due to perturbed individual VOC model species. Noted that HDDM approach was only used in experiment S3-S5 which involves calculation of higher order sensitivity, while DDM approach was used in all other experiments and in conjunction with PMF analysis.

295

Table 1: Perturbed emissions considered in the 25 sensitivity tests. The first 5 sensitivity tests S1-S5 accounts for the first-order, second-order and cross-order sensitivity due to the domain-wide NO_x and VOC emissions and the other 20 sensitivity tests S6-S25 accounts for the individual VOC model species.

Exp	Perturbations	First-order sensitivity	Second-order sensitivity
S1	∂NO_x	NO _x emissions	-
S2	∂VOC	VOC emissions	-
S3	$\partial^2\text{NO}_x$	-	NO _x emissions
S4	$\partial^2\text{VOC}$	-	VOC emissions
S5	$\partial\text{NO}_x \partial\text{VOC}$	-	NO _x , VOC emissions
S6	∂ETHA	Ethane emissions	-
S7	∂PRPA	Propane emissions	-
S8	∂PAR	Paraffins emissions	-
S9	∂ETH	Ethene emissions	-
S10	∂ISOP	Isoprene emissions	-
S11	∂TER	Monoterpene emissions	-
S12	∂OLE	Terminal olefins emissions	-
S13	∂IOL	Internal olefins emissions	-
S14	∂FORM	Formaldehyde emissions	-
S15	∂ALD2	Acetaldehyde emissions	-
S16	∂ALDX	Higher acetaldehyde emissions	-
S17	∂ACET	Acetone emissions	-
S18	∂KET	Ketone emissions	-
S19	∂ETHY	Acetylene emissions	-
S20	∂ETO	Ethanol emissions	-
S21	∂MEOH	Methanol emissions	-
S22	∂BENZ	Benzene emissions	-
S23	∂TOL	Toluene emissions	-
S24	∂XYL	Xylene emissions	-
S25	∂NAPH	Naphthalene emissions	-

300 2.4 Positive Matrix Factorization (PMF) Model

Positive matrix factorization (PMF) model is a source-receptor statistical factor analysis method, widely used for apportioning sources of air pollution and resolves the dominant factor profile without prior knowledge of sources; the

measured data uncertainty is used to optimize the model (Daellenbach et al., 2017; Fountoukis et al., 2014; Fan et al., 2021).

In this study, US EPA PMF 5.0 receptor model was used for the source apportionment of measured VOC species:

$$305 \quad x_{ij} = \sum_{k=1}^p g_{ik} f_{kj} + e_{ij} \quad (6)$$

where x_{ij} is the j -th species concentration measured in the i -th sample, g_{ik} is the airborne mass contribution from the k -th source in the i -th sample, f_{kj} is the j -th species fraction to the k -th source and e_{ij} is the residual associated with the j -th species concentration measured in the i -th sample. p is the total number of independent sources. Noted that the subscript “ i ” in Eq. (6) refers to the i -th sample which is different from Eq. (1-5) that refers to the emission of i -th species. In the source parsing

310 process, the objective function Q is solved with an iterative minimization algorithm. The objective function is defined as:

$$Q = \sum_{i=1}^n \sum_{j=1}^m \frac{x_{ij} - \sum_{k=1}^p g_{ik} f_{kj}}{u_{ij}} \quad (7)$$

where u_{ij} is the uncertainty of j -th species in i -th sample.

Figure 4 shows the overall framework of the PMF source apportionment methodology. The data used to drive the PMF
 315 model source apportionment was obtained from Taiwan’s Photochemical Assessment Monitoring Stations (PAMS); details of the PAMS location and sampling protocol are provided in the supplementary material. Species with >55% of samples missing data or below MDL were discarded (Chen et al., 2019; Wu et al., 2016). Among 54 PAMS-VOC species, a total of 16 species were discarded due to abundant missing data, but had a low OFP (Figure S5). The sample data uncertainty is calculated using:

$$320 \quad unc = \begin{cases} 5/6 \times MDL & , x_{ij} < MDL \\ \sqrt{(\sigma \times x_{ij})^2 + (0.5 \times MDL)^2} & , x_{ij} \geq MDL \end{cases} \quad (8)$$

where MDL represents the minimum detection limit, σ is the error fraction (i.e. 10% was used in this study), and x_{ij} is the concentration of j -th species in i -th sample. In the PMF, we tested a range of 3-8 VOC sources to determine the optimal number. Details of this protocol will be discussed further below.

325 The Taiwan PAMS data provided a total of 54 VOC species, but not all species were used for the PMF model due to an abundance of values below MDLs. Among the selected 38 VOC species (n=744 samples), they were further categorized into three categories: strong, weak and poor according to two steps. The first step calculated the signal-to-noise ratio (S/N) where species with a S/N value less than 0.5 were classified as poor and removed from the PMF model. This threshold value 0.5 was determined according to the EPA PMF v5.0 user guide and also recommended by other PMF studies (Rajput et al., 330 2016; Reff et al., 2007). Next, we performed the model base run and calculated the correlation between the modeled and measured concentration for each species. In this step, species with a correlation value ≥ 0.6 were classified as 'strong' and otherwise as 'weak', which were then down-weighted by tripling the analytical uncertainty (Pallavi et al., 2019; Chen et al., 2019). Details of the species categorization is summarized in Table 2. Finally, a total of 21 VOC species were identified and used in the PMF source apportionment analysis, which accounted for 75.0%, 76.4% and 76.1% of the total VOC 335 concentrations in CZ, QT and XG, respectively.

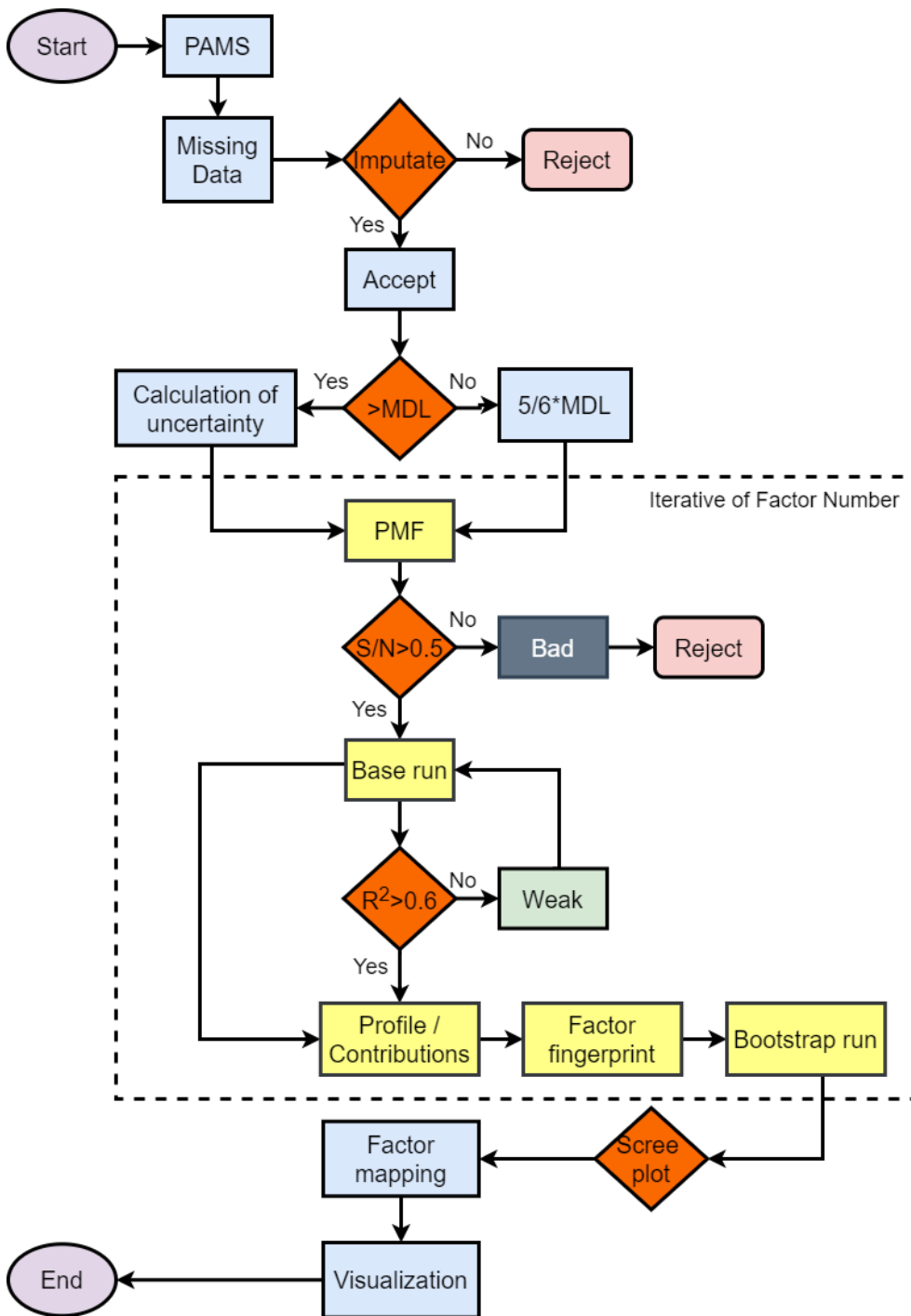


Figure 4: Overall framework of the Positive Matrix Factorization (PMF) model methodology. Processes in the dashed-line box are repeated for 3-8 factor number combinations. MDL: minimum detection limit.

340 Table 2: Categorization of PAMS-VOC species for PMF model source apportionment analysis. Grey-highlighted species represents unused species with abundant missing data >55% below minimum detection limit (MDL). Poor category species are identified for low S/N <0.5. Weak (Strong) category species are identified for S/N \geq 0.5 and $R^2 < 0.6$ ($R^2 \geq 0.6$) between measured and modelled concentration predicted by PMF model. Both unused and bad species are removed from PMF model analysis.

No	VOC Species	Chaozhou		Qiaotou		Xiaogang	
		MDL	Category	MDL	Category	MDL	Category
1	Ethane	Yes	Strong	Yes	Weak	Yes	Strong
2	Ethylene	Yes	Weak	Yes	Weak	Yes	Weak
3	Propane	Yes	Strong	Yes	Strong	Yes	Weak
4	Propylene	Yes	Weak	Yes	Weak	Yes	Weak
5	Isobutane	Yes	Strong	Yes	Weak	Yes	Strong
6	n-Butane	Yes	Strong	Yes	Weak	Yes	Strong
7	Acetylene	Yes	Strong	Yes	Weak	Yes	Strong
8	t-2-Butene	Yes	Poor	Yes	Poor	Yes	Poor
9	1-Butene	Yes	Poor	Yes	Poor	Yes	Poor
10	cis-2-Butene	No	-	No	-	No	-
11	Cyclopentane	Yes	Poor	Yes	Poor	Yes	Poor
12	Isopentane	Yes	Strong	Yes	Weak	Yes	Strong
13	n-Pentane	Yes	Strong	Yes	Weak	Yes	Weak
14	t-2-Pentene	No	-	No	-	No	-
15	1-Pentene	No	-	No	-	No	-
16	cis-2-Pentene	No	-	No	-	No	-
17	2,2-Dimethylbutane	No	-	No	-	No	-
18	2,3-Dimethylbutane	Yes	Poor	Yes	Poor	Yes	Poor
19	2-Methylpentane	Yes	Poor	Yes	Poor	Yes	Poor
20	3-Methylpentane	Yes	Poor	Yes	Poor	Yes	Poor
21	Isoprene	Yes	Strong	Yes	Strong	Yes	Strong
22	n-Hexane	Yes	Weak	Yes	Weak	Yes	Weak
23	Methylcyclopentane	Yes	Poor	Yes	Poor	Yes	Poor
24	2,4-Dimethylpentane	No	-	No	-	No	-
25	Benzene	Yes	Weak	Yes	Weak	Yes	Weak
26	Cyclohexane	Yes	Weak	Yes	Weak	Yes	Weak
27	2-Methylhexane	Yes	Poor	Yes	Poor	Yes	Poor

28	2,3-Dimethylpentane	No	-	No	-	No	-
29	3-Methylheptane	No	-	No	-	No	-
30	2,2,4-Trimethylpentane	Yes	Strong	Yes	Weak	Yes	Strong
31	n-Heptane	Yes	Poor	Yes	Poor	Yes	Poor
32	Methylcyclohexane	Yes	Poor	Yes	Poor	Yes	Poor
33	2,3,4-Trimethylpentane	Yes	Poor	Yes	Poor	Yes	Poor
34	Toluene	Yes	Weak	Yes	Strong	Yes	Strong
35	2-Methylheptane	No	-	No	-	No	-
36	3-Methylhexane	Yes	Poor	Yes	Poor	Yes	Poor
37	n-Octane	Yes	Poor	Yes	Poor	Yes	Poor
38	Ethylbenzene	Yes	Strong	Yes	Strong	Yes	Weak
39	m,p-Xylene	Yes	Strong	Yes	Strong	Yes	Weak
40	Styrene	No	-	No	-	No	-
41	o-Xylene	Yes	Strong	Yes	Strong	Yes	Weak
42	n-Nonane	No	-	No	-	No	-
43	Isopropylbenzene	Yes	Weak	Yes	Weak	Yes	Weak
44	n-Propylbenzene	Yes	Poor	Yes	Poor	Yes	Poor
45	m-Ethyltoluene	Yes	Weak	Yes	Strong	Yes	Strong
46	p-Ethyltoluene	Yes	Poor	Yes	Poor	Yes	Poor
47	1,3,5-Trimethylbenzene	No	-	No	-	No	-
48	o-Ethyltoluene	Yes	Poor	Yes	Poor	Yes	Poor
49	1,2,4-Trimethylbenzene	Yes	Weak	Yes	Strong	Yes	Weak
50	n-Decane	No	-	No	-	No	-
51	1,2,3-Trimethylbenzene	Yes	Poor	Yes	Poor	Yes	Poor
52	m-Diethylbenzene	No	-	No	-	No	-
53	p-Diethylbenzene	No	-	No	-	No	-
54	n-Undecane	No	-	No	-	No	-

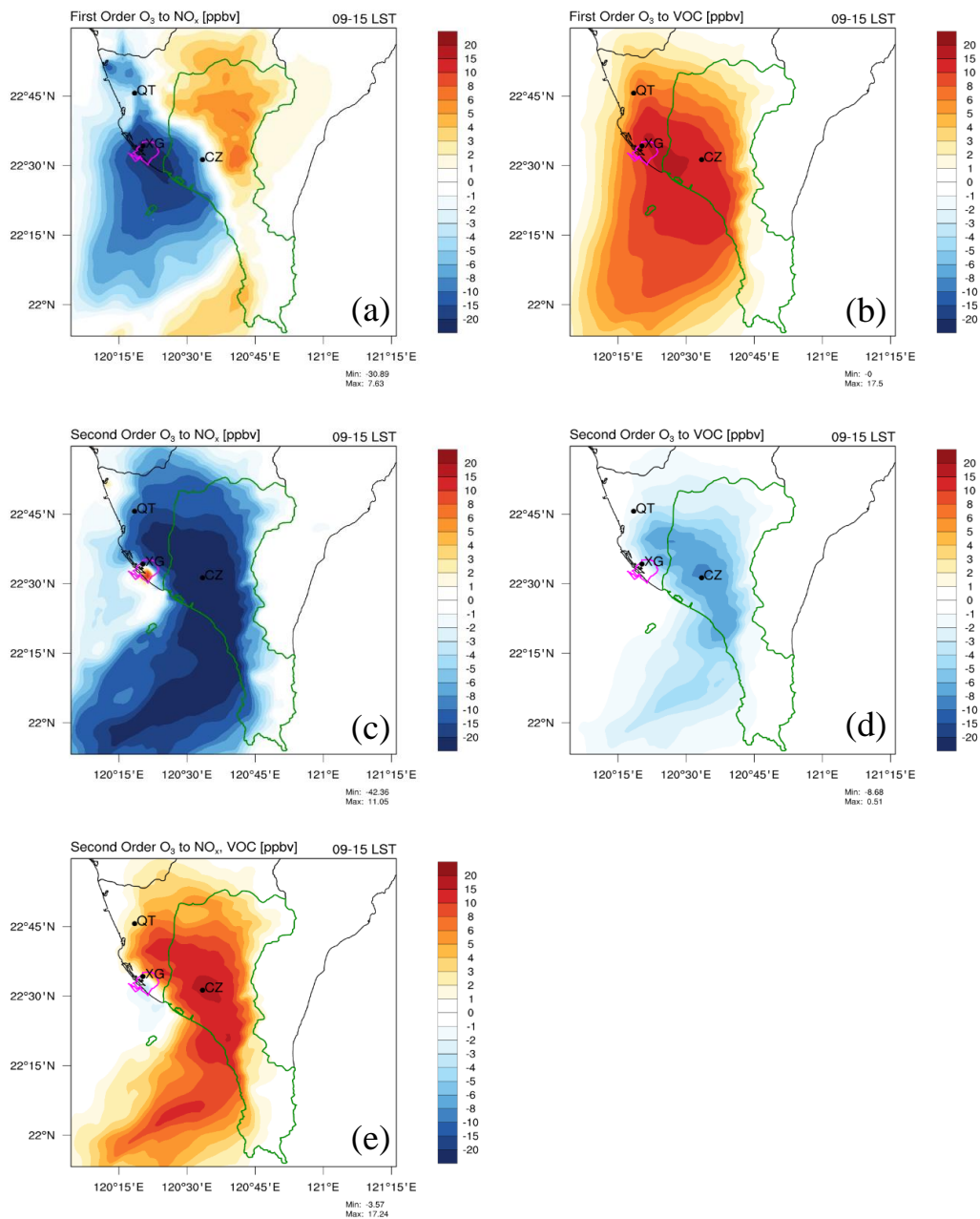
345

3. Results & Discussions

3.1 Decomposition of Ozone Response

First-order sensitivity coefficients indicate the linear response of ozone concentrations to small changes in emissions. Ozone response to small changes of daytime (09-15 LST) NO_x emissions is dominated by negative sensitivities (VOC-limited) in the urban area and positive sensitivities (NO_x-limited) in the inland area near the mountainous region (Figure 5(a)). Small areas of extreme negative sensitivity were concentrated near the most intense NO_x emissions in XG (magenta borderline in

Figure 5), a heavy industrial park district in the study domain. Although high VOC emissions are also present in the industrial park, the magnitude of first-order sensitivity to NO_x emissions (-31 ppb h^{-1}) is relatively larger than that of VOC emissions ($+18 \text{ ppb h}^{-1}$), indicating that O_3 linear response to NO_x emissions is proportionally greater than that of VOC emissions from the industrial park (see Figure 5(a, b)). Moving away from the source emissions, the negative sensitivity to daytime NO_x emission gradually increases and becomes positive in inland area, indicating the shift of ozone production sensitivity from a VOC-limited to NO_x -limited regime. The negative sensitivities to daytime NO_x emissions extend to the coastal Pingtung county (green borderline in Figure 5), reflecting the downwind transport of NO_x from the source region by the steering of northeasterly winds to westerly winds from the terrain effect and local circulation. Areas of positive sensitivity to VOC emissions overlap with areas of negative sensitivity to NO_x emissions, confirming the VOC-limited regime, but also extend to NO_x -saturated areas. The larger area of VOC sensitivities could also be explained by the longer atmospheric lifetime of VOCs (hours to days for high OFP species such as toluene, ethylbenzene, xylene, ethane, and ethylene) as compared to NO_x (1.0-4.5 hours) (Laughner and Cohen, 2019).



365 Figure 5: CMAQ-HDDM first-order sensitivity coefficient of O_3 to (a) NO_x emissions, (b) VOC emissions, second-order sensitivity coefficient of O_3 to (c) NO_x emissions, (d) VOC emissions, (e) second-order cross sensitivity coefficients of O_3 to NO_x , VOC emissions, at daytime 09-15 LST averaged during the entire simulation period. Magenta and green highlighted borderline represents Xiaogang District and Pingtung region, respectively.

370 Second-order sensitivity indicates the responsiveness of ozone concentration to broader changes in emissions and also delineates the non-linear sensitivities of ozone concentration to emissions. Most of the urban areas (except XG, an industrial park) exhibited negative second-order sensitivities to daytime NO_x emissions, which when coincident with negative first-order sensitivities yields a negative O_3 convex response: urban O_3 increases linearly but decreases non-linearly with decreasing NO_x emissions. Thus, in these areas, the large negative second-order sensitivities countered the linear negative

375 sensitivity of O_3 creating urban O_3 production conditions that were less sensitive than otherwise to changes in NO_x emissions. In contrast, positive second-order sensitivities to daytime NO_x emissions in XG were coincident with negative first-order sensitivities, which yielded a negative O_3 concave response with linear and nonlinear O_3 increases during decreasing NO_x emissions (Fig. S2). This concave O_3 response is also observed in the Chicago O'Hare (ORD) area, which is highly polluted and severely impacted by aircraft emissions (Arter and Arunachalam, 2021); it is similar to XG where it also

380 hosted an international airport and several industrial parks. In XG, the NO_x titration effect that consumes ozone is relatively higher than other urban areas of Kaoping due to the high NO_x/VOC condition (see Figure S6) and hence a rapid reduction in NO_x level could further suppress the titration effect and increase the ozone formation rate. While for urban areas outside of XG, rapid NO_x reductions push the condition into transition or NO_x -limited regime and suppression of the titration is countered by less efficient O_3 production. Cross sensitivities indicate the interaction effects of the sensitivities when both

385 NO_x and VOC emissions are changed simultaneously (limited to NO_x and VOC changes in the same direction, positive or negative). In most cases, decreasing the NO_x (VOC) emissions enhanced the sensitivities of ozone to the limiting precursors, NO_x (VOC) due to the positive cross-sensitivity of ozone to NO_x and VOCs (see Figure 5e). Cross-sensitivities also indicate how results from emission control strategies may change from summing the results of decreasing individual NO_x and VOC emissions (Arter and Arunachalam, 2021). Cross-sensitivities usually have only a small contribution in highly VOC-limited

390 or highly NO_x -limited conditions because the associated net ozone production rates are driven singly either by VOC or NO_x , respectively (Sillman, 1999; Cohan et al., 2005). This result is reproduced in our model simulation; low cross-sensitivities between NO_x and VOC are simulated in XG (highly VOC-limited condition) as well as remote areas in west side of the mountain range in the southern Taiwan (highly NO_x -limited condition), while high positive cross-sensitivities between NO_x

and VOC emissions are concentrated in downwind suburban areas (e.g. Pingtung county) (Figure 5e). The latter result
395 highlights a potential under-prediction of O₃ formation sensitivity if the cross-sensitivity term is excluded in suburban areas.

3.2 Taylor-series Expansion Approximation

We then sought to exploit the sensitivity coefficients determined above to estimate the impact of NO_x and VOC emission
reductions on ozone concentrations in southern Taiwan from the time of our study period, 2018 to 2025. To determine the
400 level of emissions reduction in the near term, we referred to the long-term trend of projected emissions in Taiwan as reported
in the Taiwan Emission Data System (TEDS 11.0; <https://air.epa.gov.tw>), which estimated an overall reduction of 53%
(NO_x) and 14% (NMHC) over 22 years (2007-2028). In recent years, the decreasing trends for both NO_x and NMHC
emissions have slowed down (see Figure S7). We then used 5% emission reductions over the 8-year near-term period from
2018-2025 as a conservative estimate. Although this reduction is small, the Taylor-series approximation (Eq. 4-5) considers
405 the first-order, second-order and cross sensitivity coefficients of O₃ to this change in NO_x and VOC emissions and provides a
clearer picture on how O₃ will change with a parallel reduction in emissions in the near future.

We estimated the ozone concentration at different scenarios represented by different emission control strategies for the
typical seasonal transition period already simulated above, which often causes high O₃ episodes in the study area. For
410 simplicity, reduction of domain-wide NO_x and VOC emissions is considered. Given the high nonlinearity of the ozone
response to emissions of NO_x and VOC, the Taylor Series approximation is necessary to consider the higher order terms
involved in second-order and cross-term sensitivity of NO_x and VOC emissions. To compare a series of targeted emission
control strategies, four experiments are considered: (1) baseline, (2) NO_x control, (3) VOC control, and (4) NO_x & VOC
control. All experiments reduce the targeted emission by 5% except for the baseline experiment representing the current
415 emission with no perturbations. Figure 6 shows the baseline O₃ concentration and its corresponding response to NO_x control,
VOC control, and NO_x & VOC control at daytime 12 LST. Benefits of NO_x control (i.e. reduction of O₃ by 0.6-0.8 ppbv) are
seen to dominate over the inland area. However, an adverse effect of increased O₃ concentration >1.8 ppbv from NO_x control
is simulated near the western coastal urban area where high NO_x emissions are concentrated. This agrees with our previous

analysis that urban O_3 concentrations are estimated to increase from decreasing NO_x emissions for most of the urban areas
420 that follow O_3 concave sensitivity behaviors and increase more for highly polluted urban areas (i.e. XG) that follows O_3
convex sensitivity behaviors. In contrast, no adverse effect is observed from VOC control, but rather resulted in decreased O_3
concentration over much of the study region. The largest ozone response to VOC control is -1.4 ppbv in the urban area, but
also extended to the inland area. Control of both NO_x and VOC emissions resulted in reduced inland O_3 concentration, a
marginal difference in urban areas, and slightly increased O_3 concentration near the large point source area in XG.

425

The decreasing trend of NO_x emission in the future is likely to continue owing to adoption of electric vehicles (EV), which
may impact the urban and inland areas differently due to the respective sensitivity regime. Using the Taylor-series
approximation, we estimated ∂O_3 against ∂VOC emissions at different levels of projected ∂NO_x emissions for Xiaogang, XG
(urban) and Chaozhou, CZ (inland) at 12:00 LST (Figure 7). Projected ∂NO_x emissions at 0% (black line) and -5% (red line)
430 represents the current year 2018 and near future 2025, respectively while other projected ∂NO_x emissions at arbitrary -50%
(blue), -25% (magenta), and +25% (green) are presented for alternative scenarios. At CZ, our results show that inland O_3
becomes less sensitive to varying ∂VOC emissions (i.e. less benefits of VOC control) at greater reductions of ∂NO_x emission
at -25% and -50% (i.e. moving into the NO_x -limited regime). On the other hand, ∂O_3 at XG is always sensitive to varying
levels of ∂VOC emissions at all levels of ∂NO_x scenarios and ∂O_3 increases in parallel following the ∂NO_x order -50%, -25%
435 and -5%. This is expected in a highly polluted area that favors VOC-limited conditions where O_3 could have the reverse
effect to NO_x due to the reduced titration effect for decreasing NO_x . Besides, at all projected levels of ∂NO_x emissions, urban
 O_3 continues to decrease with decreasing VOC emissions. We showed in the Taylor-series approximation analysis when we
hypothetically reduce NO_x emission at arbitrary -50% and -25% scenario, which should expect an improvement in the
overestimation of NO_2 , urban O_3 at XG remains in a VOC-limited condition. Therefore, it is certain that the VOC-limited
440 condition at urban areas of southern Taiwan is mainly due to the high anthropogenic NO_x emissions and VOC controls are
beneficial in reducing O_3 concentration in highly polluted urban areas.

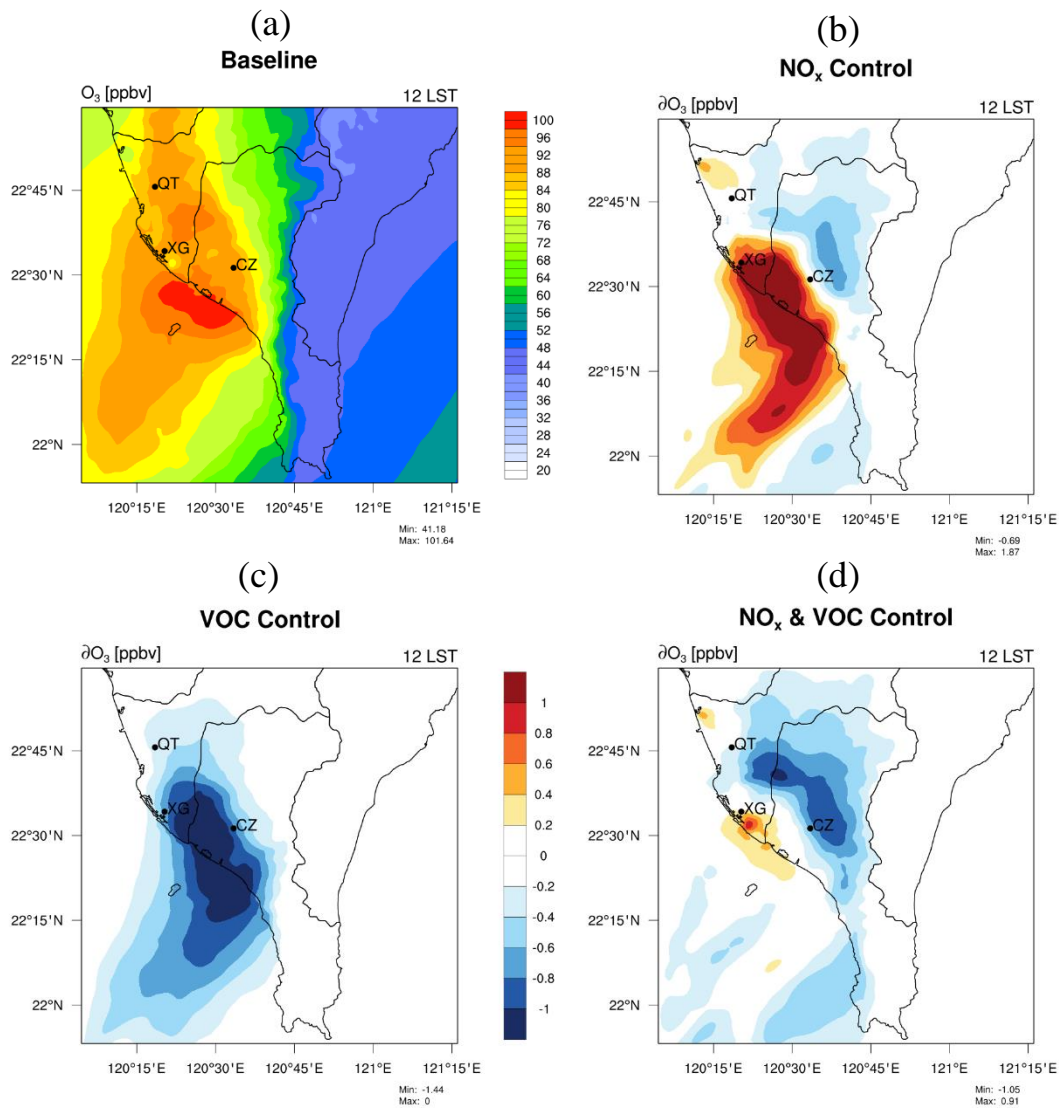


Figure 6: Spatial distribution of O₃ concentration in (a) baseline with no perturbations in NO_x and VOC emissions, and 445 changes in O₃ concentration under (b) NO_x control scenario, (c) VOC control scenario, and (d) NO_x & VOC control scenario at daytime 12 LST. All scenarios reduced the targeted emissions by 5% except for the baseline.

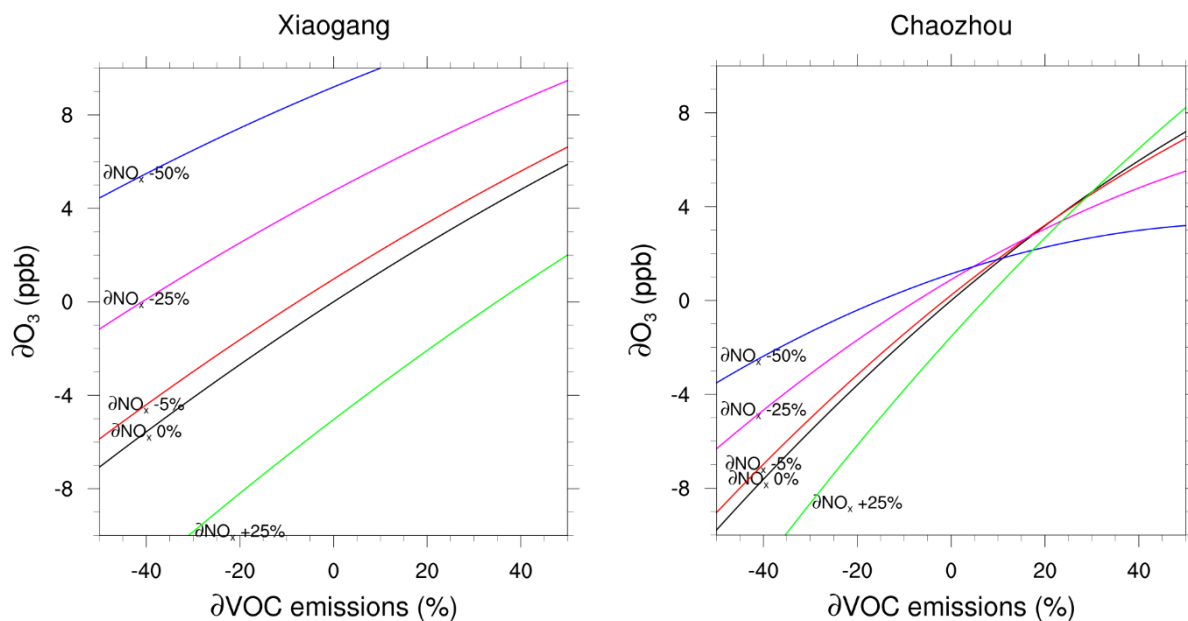


Figure 7: Taylor-series approximation of ∂O_3 against ∂VOC emissions at different level of projected ∂NO_x emissions for Xiaogang (urban) and Chaozhou (inland) averaged at 12:00 LST. Projected ∂NO_x emissions at 0% (black line) and -5% (red line) represents the current year 2018 and near future 2025, respectively; other projected ∂NO_x emissions at arbitrary -50%, $\pm 25\%$ are presented for far-future comparison purpose.

3.3 Sensitivity of Individual Modeled VOC Species

In this subsection, we further evaluate the sensitivity of the ozone response to individual modeled VOC emissions using the CMAQ direct decoupled method (DDM-3D). Note that only the first-order sensitivity coefficient of individual VOC species in CB6 is calculated considering the high computational cost and the second-order sensitivity coefficients of ozone to total VOC emissions have a low contribution. A total of 20 individual sensitivity tests were performed to target each modeled lumped VOC class or individual species (refer to Table 1 for a complete list of modeled VOC species). Figure 8(a) shows the daytime CMAQ DDM sensitivity coefficient of ozone to the VOC emissions, arranged in ascending order and separated for urban and inland area. The urban area sensitivity coefficients are substantially higher than that in the inland area for all species, which is expected due to the VOC-limited regime in the urban area. Among the 20 VOC species, the six most

important VOC species were identified as XYL (xylene), OLE (terminal C-C olefins), PAR (paraffins), ETH (ethene), TOL (toluene), IOL (internal C-C olefins).

465

XYL and TOL are aromatic hydrocarbons that are included in the BTEX group, along with benzene and ethylbenzene. The ranking of BTEX with respect to ozone formation potential in a high NO_x environment is often done using maximum incremental reactivity (MIR), which uses unitless coefficients and indicates the amount contributed to ozone formation in the air mass by individual compounds. Based on the MIR scale adopted from the literature (Atkinson, 1997; Carter, 1994), m,p-
470 xylene (8.20) are the most dominant contributors to ozone formation among BTEX, followed by toluene (2.70), ethylbenzene (2.70) and benzene (0.42). Our result agrees with the MIR scale, which yielded classifications of XYL and TOL as the second and fifth most sensitive VOC species to O_3 among the 20 VOC species considered in the sensitivity tests. Other sensitive VOC species to O_3 formation include alkanes (i.e. PAR (MIR = 0.32)) and alkenes (i.e. OLE (8.24), ETH (4.37), IOL (13.11)).

475

To gain additional insights on the ozone response to the six most sensitive VOC species, we grouped them into three categories (i.e. alkenes: OLE, ETH, IOL; aromatics: TOL, XYL; alkanes: PAR) and plotted the spatial distributions of the sensitivities at 12 LST (Figure 8(b-d)). The sensitivity of ozone to alkenes and alkanes have a similar pattern with higher sensitivity concentrated near the emission source and slightly shifted towards inland/mountainous and Pingtung county due
480 to the local circulation and the prevailing northeasterly winds. For the sensitivity of ozone to aromatics, the spatial distribution has a smaller area coverage and higher sensitivity is more concentrated near the emission source. To render a clearer picture on the spatial distribution of O_3 sensitivity to each VOCs component, the spatial distribution of some highly sensitive VOC component emissions (i.e. XYL, OLE, PAR, ETH, TOL, IOL) are provided in the supplementary material (see Figure S8). The role of land-sea breeze circulation in transporting the local O_3 precursors (i.e. VOC) from urban to
485 inland area is well reflected by the diurnal profile of the sensitivity coefficients (Figure 9). An obvious shift is simulated in inland area as compared to the urban area; the urban sensitivity coefficients peak at 10 LST while the peak in inland area is at 13 LST. A lag of 2-3 hours delay is mainly attributed to the daytime sea-breeze penetration that pushes the urban polluted

air towards the inland area due to the differential heating between the land and sea surfaces during the noon hours. This result also tells us that VOC emissions from urban area are largely responsible for the inland high ozone episodes.

490

Using an approach similar to OFP, we quantified the relative ground-level ozone impacts of the six most sensitive VOC species by multiplying the MIR coefficients to its corresponding concentrations at 12 LST (see Figure 8(e-g)). Due to the abundance of PAR, OFP calculated for alkanes emission is significant over the western coastal region of southern Taiwan. The longer atmospheric lifetime of alkanes makes it more susceptible to transportation and impacting a wider area. Despite
495 alkanes having the lowest sensitivity coefficient of the six groups of VOCs in the study, the significance of alkane OFP extends over a larger area, highlighting the need for controlling alkane-related emissions to reduce the ozone pollution problem over the study area. OFP of alkenes features a point source distribution pattern indicating it is more likely related to large point source emissions. OFP of aromatics has the smallest area coverage and is highly concentrated near the populated industrial park of the study area in southern Taiwan. Among the three main contributors, aromatics have the highest maxima
500 OFP value 56 ppbv, followed by alkenes (49 ppbv) and alkanes (40 ppbv).

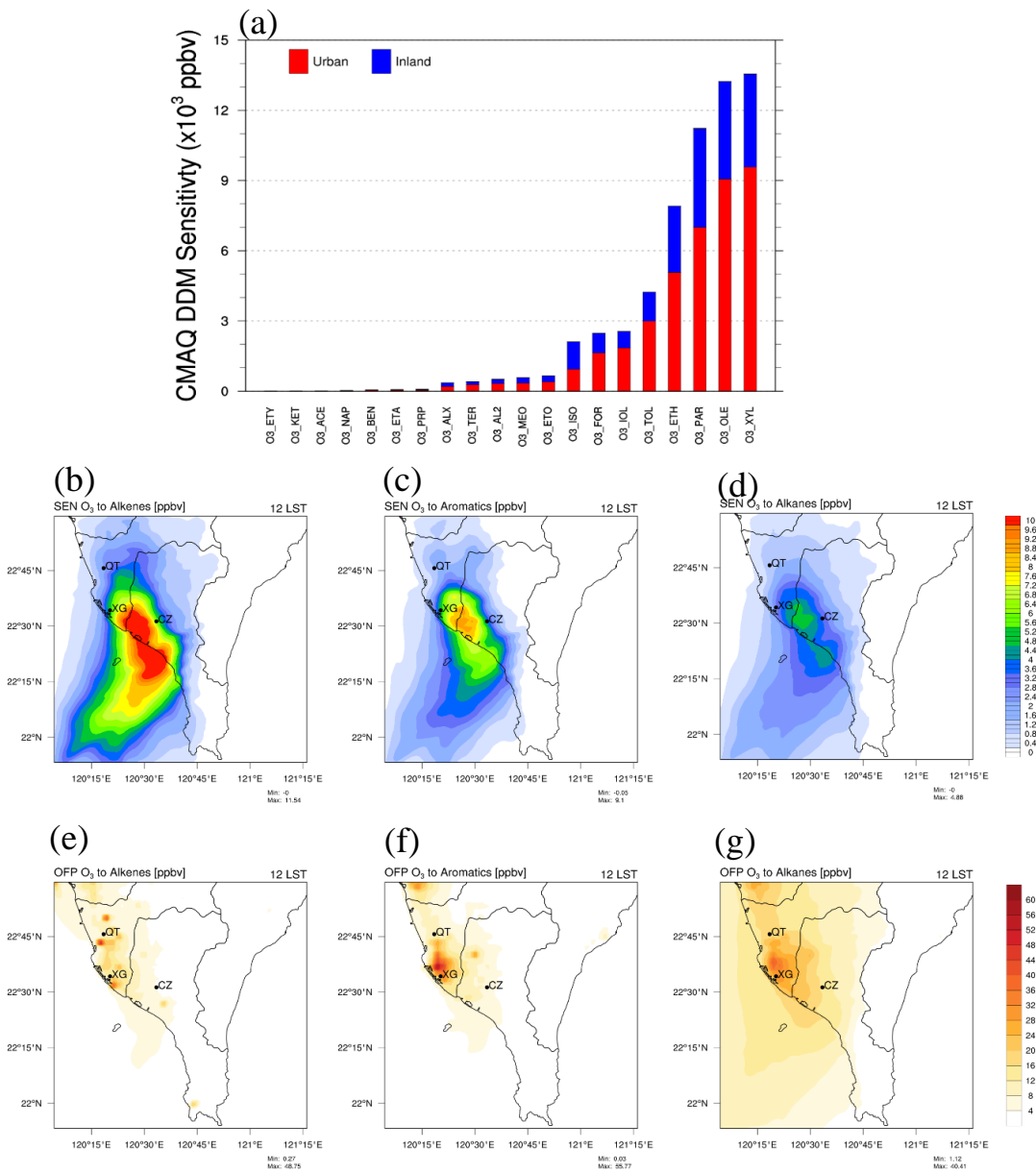


Figure 8: (a) Daily averaged CMAQ-DDM first-order sensitivity coefficient of O₃ concentrations calculated per number of grids to each modelled VOC species arranged in ascending order for urban and inland area. Sensitivity of O₃ and ozone formation potential (OFP) to (b,e) alkenes emissions (OLE + ETH + IOL), (c,f) aromatics emissions (XYL + TOL), and (d,g) alkanes emissions (PAR) at 12 LST.

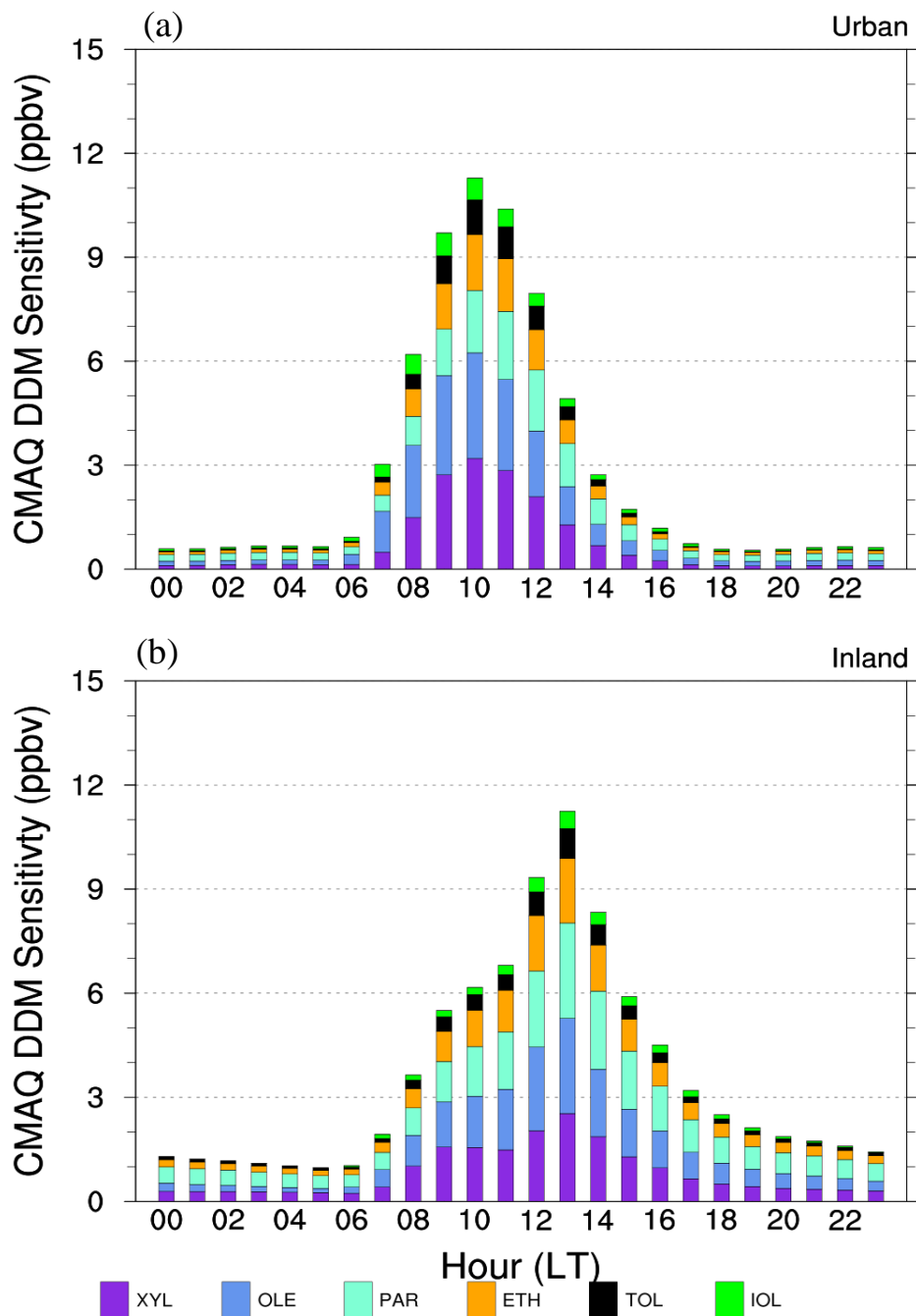


Figure 9: Diurnal variations of the CMAQ-DDM sensitivity of O₃ to the six most sensitive VOC modelled species (i.e. terminal olefins, OLE; xylene, XYL; paraffin, PAR; ethene, ETH; toluene, TOL; internal olefins, IOL) averaged for (a) urban and (b) inland area, during the entire simulation period.

Figure 10 shows the relative sensitivities for each modelled VOC to O₃ (DDM – Figure 10(a)) and its corresponding emission rate (EMIS – Figure 10(b)) averaged in urban and inland areas during the entire simulation period. Similar to the above analysis, the three main contributors were identified as alkenes (42.2% for urban; 37.1% for inland), aromatics (29.1%; 25.1%), and alkanes (18.2%; 23.4%). Other less important contributors were formaldehyde (4.1%; 3.9%), isoprene (2.3%; 5.4%), alcohols (1.9%; 2.6%) and aldehydes (0.9%; 1.6%). Due to the abundant biogenic emissions surrounding the inland area, inland ozone is more sensitive to isoprene (5.4%) as compared to the urban area. Besides, inland ozone is also more sensitive to alcohols (MEOH + ETOH) and aldehydes (ALD2 + ALDX) when compared to the urban area. This is also consistent with the higher contributions of alcohols (10.0%) and aldehydes (1.4%) inland than in urban areas (4.3% and 0.8%, respectively) (Figure 10(b)).

Overall, the DDM sensitivity tests identified three main speciated VOC groups contributing to ozone formation, namely alkenes, aromatics, and alkanes. The six most sensitive VOC surrogates in CB6 to ozone formation in the study area are XYL, OLE, PAR, ETH, TOL, IOL in descending order. Sources of these targeted VOC species are highly variable and previous studies have attributed these species to a wide-range of emission sources not limited to traffic, industrial, petrochemical, manufacturing, solvent usage, etc. Therefore, in order to identify the sources of these VOC species for better emission control policy, source apportionment is necessary.

530

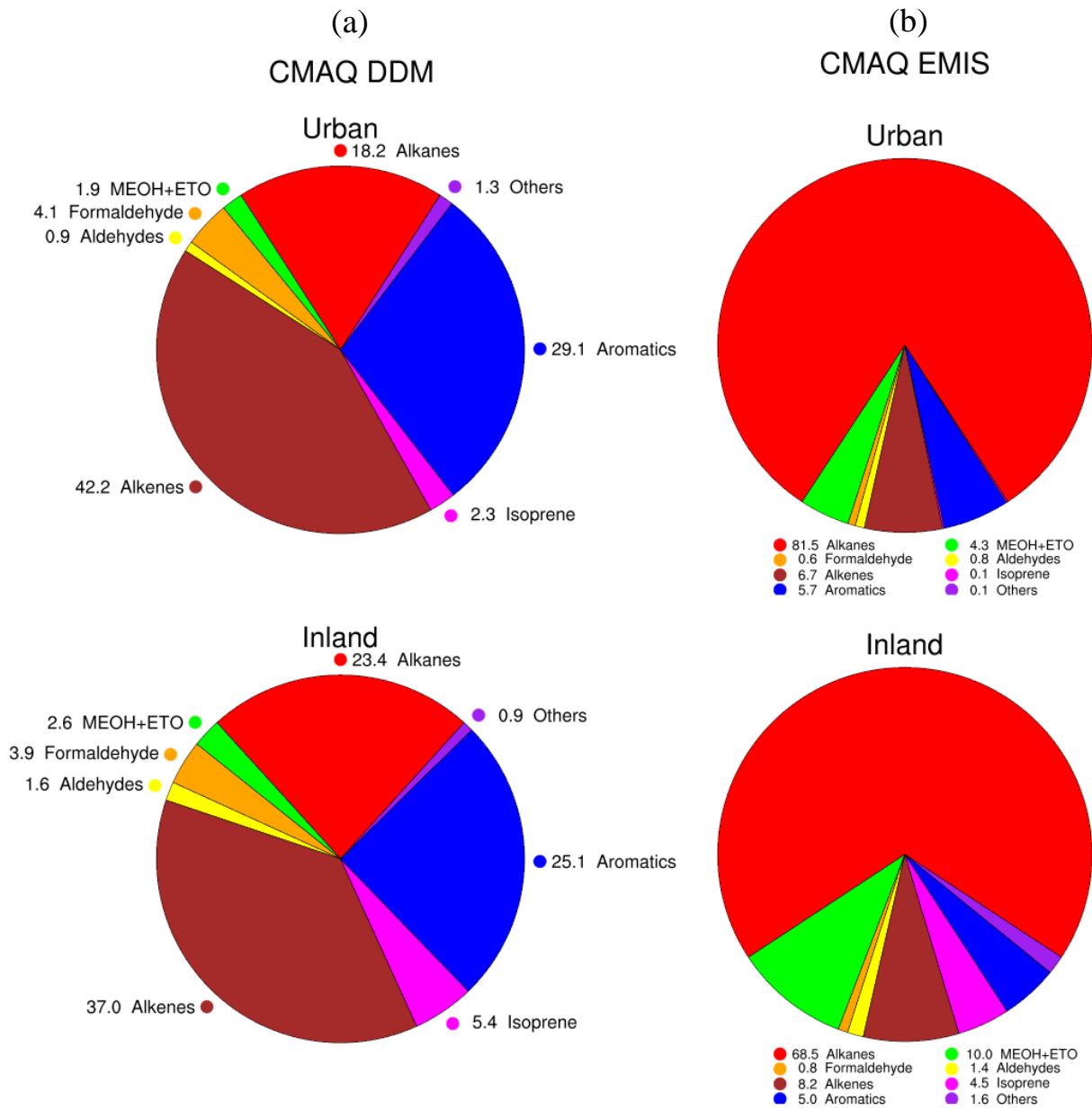


Figure 10: Relative distribution in percentage of (a) CMAQ DDM O₃ sensitivity and (b) CMAQ EMIS hydrocarbon emissions to individual VOC summed across different groups averaged for urban and inland area during the entire

535 simulation period.

3.4 Descriptive Statistics of PAMS-VOC Data & PMF Optimal Solution

In this subsection, we first describe the statistics of the PAMS-VOC data measured at Chaozhou (CZ), Qiaotou (QT) and Xiaogang (XG) which were used to drive the PMF source apportionment. CZ station is an inland station located far away from the urban core while QT and XG are urban stations. The top 15 major VOC species measured at the three PAMS stations are summarized in Table 3 and other species are shown in Figure S9. These top 15 major VOC species accounted for 65.9%, 70.7% and 68.7% of the total VOC concentrations in CZ, QT and XG, respectively. Overall, aromatics contributed the largest proportion, accounting for 117.3 ppbv (43.5%) in CZ, 312.2 ppbv (53.9%) in QT, and 361.7 ppbv (51.2%) in XG. Toluene was the most abundant VOC species in all three stations, accounting for 46.3 ± 45.0 ppbv (17.2% of total) in CZ, 140.4 ± 96.2 ppbv (24.3%) in QT, and 143.0 ± 97.7 ppbv (20.2%) in XG. Toluene is also commonly used in chemical industry (Mo et al., 2015), iron and steel industry (Nogueira et al., 2011), fuel evaporation (Wu et al., 2016), organic solvent usage (Chen et al., 2019) and a by-product of vehicle exhaust (Dai et al., 2013). The second largest contributor to total VOC concentrations were alkanes, accounting for 42.7% in CZ, 40.0% in QT, and 40.6% in XG. Among the alkanes, n-butane, propane and isopentane comprised the highest proportions, each reaching around 5% of the total VOC concentrations. n-butane isomers are emitted from a variety of sources including petroleum production and natural gas emissions (Rossabi and Helmig, 2018). In the alkenes category, ethylene and propylene are major contributors which are commonly used as raw materials in petrochemical industry and refineries. Among the three stations, the highest proportion of alkenes group is observed in XG, accounting for 7.0% of total VOCs concentrations, with 3.6% attributed to propylene.

555

560 Table 3: Concentration (mean \pm std) and proportions (%) of the top 15 PAMS-VOC species in ascending order at CZ, QT, and XG during 1-31 October 2018. Bold/italic species represents the unique species that present in the top 15 at each station. All units in ppb.

Chaozhou	Qiaotou			Xiaogang							
Species	mean	std	% Species	mean	std	% Species	mean	std	%		
Toluene	46.28	44.96	17.2	Toluene	140.39	96.21	24.3	Toluene	142.95	97.65	20.2
<i>Acetylene</i>	18.94	51.23	7.0	m,p-Xylene	49.72	28.97	8.6	m,p-Xylene	63.77	52.17	9.0
n-Butane	14.47	9.18	5.4	n-Butane	31.67	18.18	5.5	Isopentane	36.04	24.32	5.1
m,p-Xylene	13.56	11.64	5.0	Isopentane	26.81	16.41	4.6	n-Butane	33.79	19.91	4.8
Propane	13.52	7.72	5.0	Propane	23.29	10.88	4.0	Propane	26.09	18.18	3.7
Isopentane	11.25	6.38	4.2	Ethylbenzene	17.87	9.61	3.1	<i>Propylene</i>	25.51	105.81	3.6
Benzene	8.94	6.27	3.3	1,2,4-Trimethylbenzene	17.25	10.59	3.0	o-Xylene	23.29	18.34	3.3
Ethane	8.03	2.61	3.0	o-Xylene	17.18	10.18	3.0	Ethylbenzene	21.87	17.96	3.1
<i>Isopropylbenzene</i>	7.69	10.49	2.9	Benzene	16.96	9.67	2.9	1,2,4-Trimethylbenzene	20.01	15.99	2.8
Isobutane	7.30	4.23	2.7	Isobutane	14.97	7.67	2.6	Benzene	18.84	14.47	2.7
1,2,4-Trimethylbenzene	6.27	8.38	2.3	n-Pentane	11.71	11.72	2.0	n-Pentane	18.32	20.14	2.6
n-Pentane	5.66	3.81	2.1	Ethane	10.86	4.02	1.9	Isobutane	15.44	8.47	2.2
Ethylbenzene	5.44	3.98	2.0	m-Ethyltoluene	10.27	7.34	1.8	<i>Cyclohexane</i>	14.32	26.41	2.0
o-Xylene	5.20	4.28	1.9	<i>n-Hexane</i>	10.17	6.97	1.8	m-Ethyltoluene	12.85	8.76	1.8
<i>Isoprene</i>	5.14	5.02	1.9	<i>2,2,4-Trimethylpentane</i>	10.15	5.08	1.8	<i>Styrene</i>	12.30	12.77	1.7
Alkanes	114.96		42.7		231.42		40.0		286.61		40.6
Alkenes	18.33		6.8		31.41		5.4		49.37		7.0
Alkynes	18.94		7.0		3.88		0.7		9.00		1.3
Aromatics	117.32		43.5		312.18		53.9		361.69		51.2
Top 15	177.68		65.9		409.28		70.7		485.39		68.7
Total VOCs	269.55		100.0		578.89		100.0		706.67		100.0

565 Determining the number of factors is a critical step in receptor-based source apportionment methods like PMF analysis. Combinations of 3-8 sources were used to determine the optimum number of VOC sources for each PAMS station. We also calculated the uncorrelated bootstrap (BS) mapping to assist in identifying the optimum number of factors in each station. A high number of uncorrelated BS mapping indicates excessive factors are fitted in the model; therefore, this number should be kept as low as possible to avoid over-fitting. In CZ, the $Q_{\text{true}}/Q_{\text{expected}}$ was at a minimum in the 6-factor solution and the uncorrelated BS mapping was low (n=3), indicating this was the optimal solution for that site (Figure S10). Using the same protocol, the optimal solution was determined as 7 factors for QT and 5 factors for XG. Overall, a total of 8 unique factors were identified at the three stations: biogenic, solvent usage, vehicle emissions, plastic industry, manufacturing industry, mixed industry, aged air mass and motorcycle exhausts (Figure 11). The diurnal variations of the PMF factor contribution at Chaozhou, Qiaotou, and Xiaogang PAMS stations are also shown in Figure 12. Among the 8 resolved factor profiles, vehicle emissions (22%) were the largest contribution to total VOC concentrations, followed by mixed industry (21%), solvent usage

570

575

(17%), biogenic (12%), plastic industry (10%) and other factor profiles (i.e. aged air mass, motorcycle exhausts and manufacturing industry). The diurnal pattern of factor distribution of biogenic sector displays a clear diurnal cycle peak at the noontime 10-12 LST in all three stations. Meanwhile, the motor exhaust and vehicle emissions sector peak during the morning and evening traffic rush hours. The aged air mass sector is only identified in CZ and its hourly factor contribution
580 mostly existed at more stable levels when compared to other factors except for an obvious peak at 12 LST due to the sea-breeze penetration that pushes the urban polluted aged air mass towards inland area. The diurnal pattern related to industrial activity exhibits different peak hours depending on sector and station. For instance, the hourly factor contribution of solvent usage in XG has a clear bimodal peak at 10 and 16 LST; plastic industry in QT and CZ has a clear diurnal cycle peak in the noon time at 11 and 13 LST; mixed industry in QT and XG has a clear bimodal peak at 07 and 18 LST. Details of each
585 source profile and comparison with other PMF studies are discussed in Supplementary Material - Source Profiles of PMF Model.

3.5 Dominant Sources of Highly Sensitive VOC Species

We then mapped the CMAQ CB6 modeled VOC species to the PMF apportioned sources in order to identify the dominant
590 sources of highly sensitive VOC species (i.e. XYL, OLE, PAR, ETH, TOL, IOL). The dominant sources of alkene species (OLE, ETH, IOL) were identified using ethylene and propylene as tracers, sources of TOL were tracked by toluene and methyltoluene, sources of XYL were tracked by all three xylene isomers, and sources of PAR were identified using isobutane, n-butane, isopentane, n-pentane, n-hexane and 2,2,4-trimethylpentane.

595 We also developed a composite index, ψ , to quantitatively combine the CMAQ-DDM sensitivity coefficient and PMF resolved factor contribution in order to identify the key VOC species for an effective ozone abatement strategy. The index was calculated according to the j -th species and k -th source:

$$\psi_{jk} = \frac{\partial C}{\partial \varepsilon_j} \times f_{jk} \quad (9)$$

600 where C is the trace gas (O_3) concentration, ϵ is the unitless scaling factor for j emission (see Eq. 2-3), f_{kj} is the j -th species concentration to the k -th source. The first term in Eq. (9) is obtained from the CMAQ-DDM calculated first-order sensitivity coefficient where a higher value denotes greater sensitivity (extreme low sensitivity <0.01 ppb is masked out); the second term is the PMF resolved factor contribution where higher values of a particular species, j , indicate greater apportionment to the source, k . Higher values of the composite index indicate a greater priority should be given to that source-species.

605

According to the PMF source apportionment (Figure 13), the dominant source of alkene-related emissions (OLE, IOL, ETH) was attributed to mixed industry (i.e. petrochemical industry, printing industry and metal industry) (Chen et al., 2022; Pinthong et al., 2022). This source profile contributed 61.5% propylene and 47.6% ethylene in XG; 52.4% propylene and 37.9% ethylene in QT. Meanwhile, propylene and ethylene in CZ were mainly attributed to vehicle emissions and aged air masses. Given that alkene-related emissions are closely linked to large point sources (see Figure 8(e)), control of alkene emissions should focus on the mixed industry, particularly petrochemical plants. Among the three stations, the highest composite index associated with ethylene and propylene summed across all factors was obtained at XG. Though ethylene and propylene have higher sensitivities compared to other species, their composite index ($\psi_{ETHY, all k} = 5.7$ and $\psi_{PROP, all k} = 7.4$ – see Figure 13) is relatively low due to their low-abundance 11.5 ppb (1.6% of total VOCs) and 25.5 ppb (3.6%), respectively, making them less important in terms of priority.

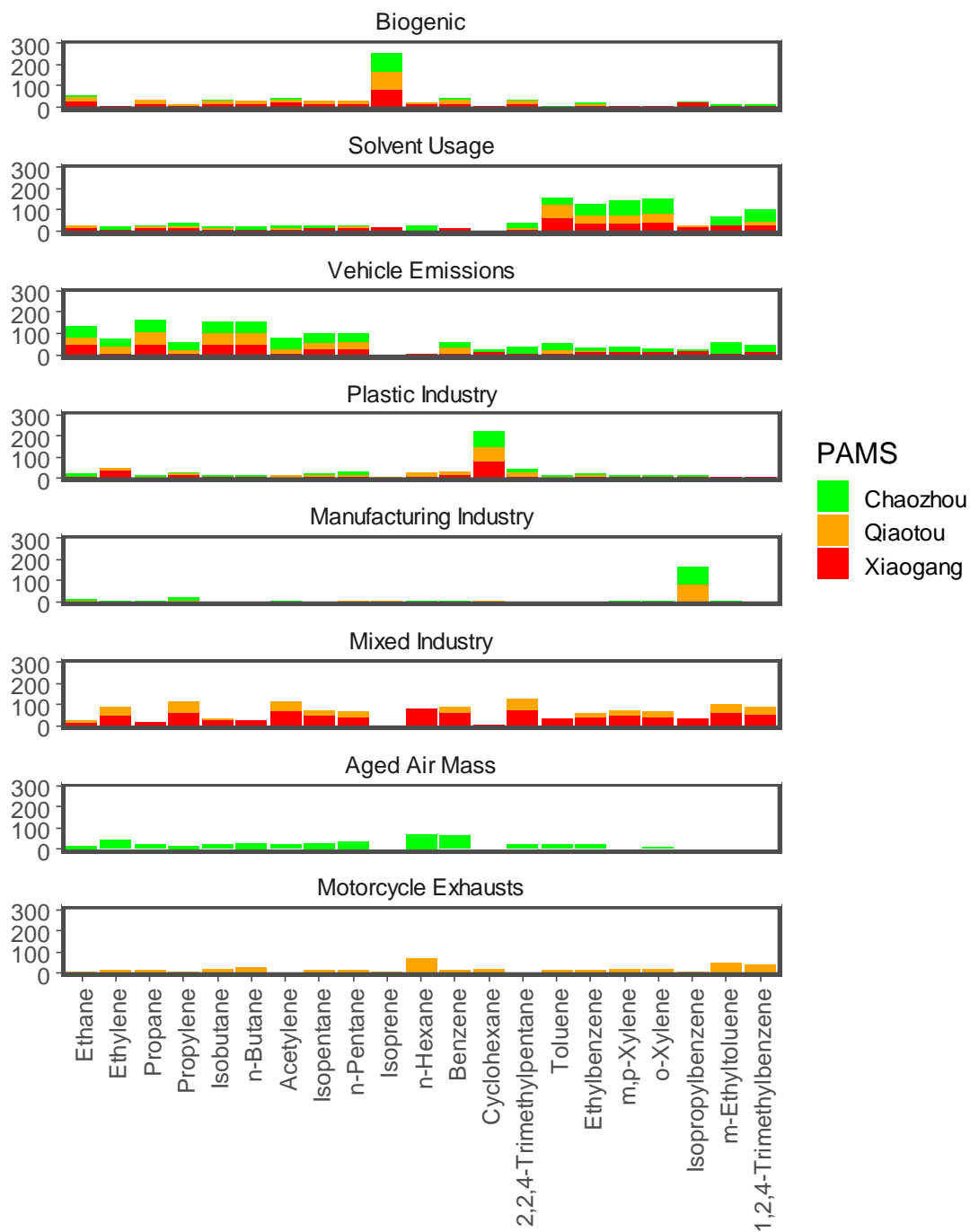
615

The highest composite index was assigned to aromatic compounds such as toluene ($\psi_{TOL, all k} = 12.1, 16.4, 53.5$ in CZ, QT and XG, respectively), m,p-xylene ($\psi_{mp-XYL, all k} = 12.0, 19.7, 53.5$), o-xylene ($\psi_{o-XYL, all k} = 4.5, 6.7, 19.0$) due to their high-abundance toluene 46.3 – 143.0 ppb (17.2 – 24.3% of total VOCs), m,p-xylene 13.6 – 63.8 ppb (5.0 – 9.0%) and o-xylene 5.2 – 23.3 ppb (1.9 – 3.3%) in all three stations (see Figure 13 & Table 3). Although toluene has much higher abundance than xylene, the composite index for both species summed across all sources is similar because the sensitivity coefficient of xylene ($\partial C/\partial \epsilon > 12$ ppb) is relatively higher than toluene ($\partial C/\partial \epsilon > 3$ ppb) (see Figure 8(a)). This indicates that emission control of both of these compounds is of high priority considering their high-abundance and high sensitivity in ozone formation. The dominant sources of aromatic-related emissions (XYL, TOL) are mainly attributed to solvent usage and

620

625 mixed industry. Solvent usage, including building coatings, paint thinners, and other products thinners (Li et al., 2021; Chen et al., 2019; Wu et al., 2016; Huang and Hsieh, 2020), contributed 64.5% xylene and 32.2% toluene in CZ; 40.6% xylene and 29.7% toluene in QT; 38.5% xylene and 43.3% toluene in XG. Mixed industry contributed 26.2% xylene and 21.9% toluene in QT; 43.5% xylene and 45.3% toluene in XG. Vehicle emissions, including motorcycle exhaust contributed less than 10% of xylene and toluene in CZ and QT. Therefore, emission control of XYL and TOL should target on solvent usage
630 particularly painting, coating, synthetic fragrances, adhesives and cleaning agents, and industrial sources in the region.

The dominant source of alkane-related emissions (i.e. PAR) is attributed to vehicle emissions in all three stations. The main tracers identified in the PMF source apportionment related to vehicle emissions are isobutane, n-butane, isopentane, n-pentane; these compounds accounted for 54.9%, 53.0%, 47.0%, and 47.0% of the PMF normalized factor contribution in CZ;
635 54.8%, 58.7%, 25.9%, and 29.1% in QT; 44.5%, 43.8%, 23.9%, and 26.8% in XG, respectively. Motorcycle exhaust also contributed to these compounds but the average contribution was relatively lower (e.g. <20% in QT). High amounts of C4-C5 alkanes (i.e. isobutane, n-butane, isopentane, n-pentane) are known indicators of traffic-related sources (Yu et al., 2021b; Huang and Hsieh, 2020; Chen et al., 2019). Among these compounds, n-butane had the highest composite index due to its high-abundance 15-34 ppb (5.1-5.5% of total VOCs). Other than freshly emitted vehicle emissions, aged air masses also
640 contributed a significant amount (~30%) to these compounds at CZ, reflecting the role of land-sea breeze circulation transporting urban vehicle plumes inland. In addition, acetylene is a well-known indicator for combustion sources and related to liquefied petroleum gas (LPG) leakage. The ratio of propane, n-butane, or i-butane to acetylene is often used to assess the domination of the LPG-vehicle sources across different cities (An et al., 2014). These ratios were 0.7, 0.8, 0.4 in CZ, 6.0, 8.2, 3.9 in QT, and 2.9, 3.8, 1.7 in XG, respectively, which were much lower than 11.5, 1.8, 2.6 in Guangzhou
645 (Zhang et al., 2013) and 11.4, 5.0, 2.3 in Mexico city (Blake and Rowland, 1995) that are heavily impacted by LPG-vehicle emissions. This indicates that there were relatively less LPG-fueled vehicles in southern Taiwan whereas LPG is merely used to fuel a gas stove for domestic household use or catering. Therefore, emission control of PAR species should focus on the gasoline-fueled vehicle emissions particularly in heavy-traffic cities.



650

Figure 11: Source profiles calculated using the PMF model at Chaozhou, Qiaotou, Xiaogang PAMS stations.

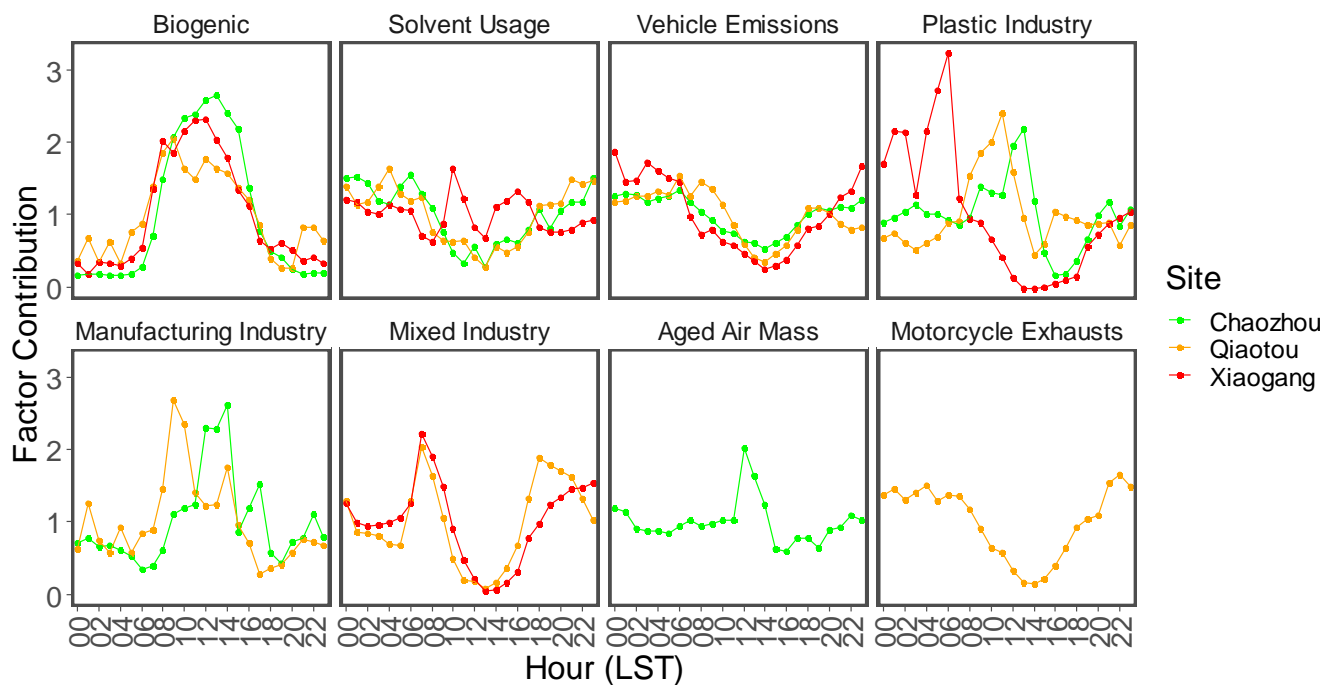


Figure 12: Diurnal variations of factor contribution calculated by the PMF model at Chaozhou, Qiaotou, Xiaogang PAMS stations

655

660

665

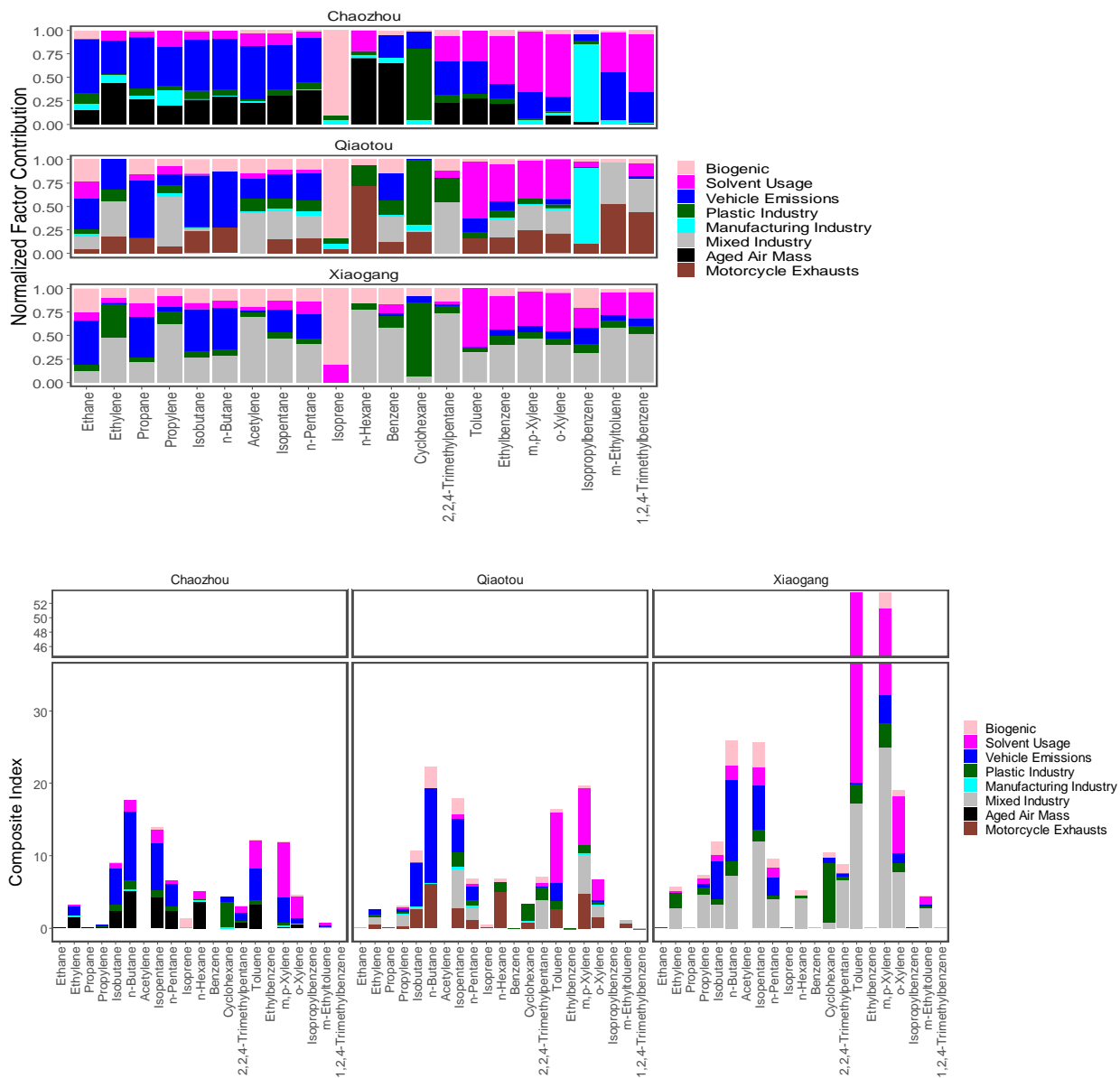


Figure 13: Normalized factor contribution and composite index of source profile to each PAMS-VOC species at Chaozhou, Qiaotou, Xiaogang PAMS station.

4. Conclusion

In this work, we used the CMAQ-DDM-3D sensitivity tool in conjunction with PMF model source apportionment to provide a comprehensive analysis of the major contributors to VOC species and the ozone formation potential (OFP) over an area of southern Taiwan. We developed a composite index that quantitatively combines the CMAQ-DDM sensitivity coefficient and PMF resolved factor contribution to identify the key VOC source-species for effective ozone abatement strategy, which is applicable to other urban areas that characterized by VOC-limited condition. A representative case in October 2018 with a daily 8-hour maxima $O_3 > 75$ ppb occurring often was the focus of this study. Low NO_x levels and high BVOC levels in the inland areas yielded a NO_x -limited regime. Although reducing NO_x emissions can reduce the inland O_3 concentrations, it could adversely increase urban O_3 due to the reduced titration effect. This is because the O_3 sensitivity production in urban area is mainly dominated by VOC-limited regime and further reducing NO_x emissions can suppress the titration effect and eventually increased the urban O_3 concentration. In contrast, control of VOC emissions is effective in urban area to reduce O_3 concentrations and has no adverse effect in rural area. Our DDM sensitivity analysis identified the six most sensitive VOC species or groups: XYL (xylene), OLE (terminal olefins), PAR (paraffins), ETH (ethene), TOL (toluene), IOL (internal olefins) in descending order, which are mainly attributed to the petrochemical industry, painting & printing industry, and vehicle emissions. Based on a composite index, effective ozone abatement strategies should prioritize (1) solvent usage such as painting, coating and printing industry that emits abundant toluene and xylene, (2) petrol vehicular emissions with high compositions of n-butane, isopentane, isobutane and n-pentane, and (3) the petrochemical industry with emphasis on ethylene and propylene.

Besides, our DDM results also highlighted the important role of formaldehyde in OFP over the study area given that it is ranked the seventh highest VOC species for O_3 sensitivity and on a per-molecule basis for O_3 sensitivity is similar to alkene (i.e. OLE, ETH, IOL) and aromatics (XYL, TOL) species. Mapping of formaldehyde to the PMF source apportionment was not done due to the lack of oxygenates in the PAMS measurement inventories. Thus, oxygenates such as FORM, ALD2, ALDX, ACET, KET along with alcohols (ETOH and MEOH) should be included in the PMF source apportionment for more complete source identification in future studies. In the current work, WRF and CMAQ are resolved at high resolution 1 km

to best represent the features of local circulations (i.e land-sea breeze, urban heat island effect) at urban scale. However, simulation at 1 km is obviously too expensive for large domain or regional modelling. The differences in HDDM and PMF analysis between D03 (3 km) and D04 (1 km) due to grid resolution remain an open question which deserves future in-depth investigations. Although the performance of the simulated meteorological parameters (T2, WS, and WD) at both urban and rural stations are acceptable in the benchmark recommended by USEPA, notable differences in temperature (underestimation) and wind speed (overestimation) are still observable in our simulation work. These biases could be susceptible to underestimation in photochemical ozone production due to the fictitious cold bias and enhanced dispersion. Therefore, careful treatment on the urban-scale data assimilation in temperature, wind field and relative humidity are recommended in future to improve the model prediction.

705

Other important findings obtained in this study are summarized below:

- Negative (positive) first-order sensitivities to daytime NO_x emissions are dominant in urban (inland) area, indicating ozone production sensitivity favors the VOC-limited regime (NO_x -limited regime). Negative sensitivities are also extended to some parts of the coastal area of Pingtung county, reflecting the downwind transport of the urban NO_x by the steering northeasterly winds due to the terrain effects and local circulations.
- Most of the urban areas (except Xiaogang, an industrial park) exhibited negative first-order and second-order sensitivities to daytime NO_x emissions, indicating a negative O_3 convex response. However, due to the large negative second-order sensitivities, the urban O_3 increases from the linear effect are largely attenuated by the non-linear effect. As a result, urban O_3 becomes less sensitive to changes in NO_x emissions but more sensitive to VOC emissions which favors the VOC-limited conditions.
- Based on the PMF model source apportionment, a total of 8 factor profiles are identified as mixed industry (21%), vehicle emissions (22%), solvent usage (17%), biogenic (12%), plastic industry (10%), aged air mass (7%), motorcycle exhausts (7%), and manufacturing industry (5%).

715

- Benefit of VOC control in inland areas is expected to reduce gradually when NO_x emissions continue to decrease over the long-term but control of VOCs in highly polluted urban areas remains effective despite a large reduction in NO_x in the future.

Code/Data Availability

The code of the WRF software was obtained from <https://www2.mmm.ucar.edu/wrf/users/download/>. The code of the CMAQ software was taken from <https://github.com/USEPA/CMAQ/>. The FNL data were adopted from <https://rda.ucar.edu/datasets/>. The Positive Matrix Factorization Model for Environmental Data Analyses was obtained from <https://www.epa.gov/air-research/positive-matrix-factorization-model-environmental-data-analyses>. The observational data of surface meteorology, air pollutant and photochemical assessment monitoring stations (PAMS) were provided by Taiwan Environmental Protection Agency (TEPA) at <https://www.epa.gov.tw>.

Author Contribution

Jackson Hian-Wui Chang: Conceptualization, Methodology, Investigation, Formal analysis, Validation, Software, Writing - Original Draft. *Stephen M. Griffith*: Visualization, Writing- Reviewing and Editing. *Steven Soon-Kai Kong*: Formal analysis, Software. *Ming-Tung Chuang*: Formal analysis, Software. *Neng-Huei Lin*: Visualization, Funding acquisition, Writing- Reviewing and Editing.

Competing Interests

The authors declare that they have no conflict of interest

References

An, J., Zhu, B., Wang, H., Li, Y., Lin, X., and Yang, H.: Characteristics and source apportionment of VOCs measured in an industrial area of Nanjing, Yangtze River Delta, China, *Atmos Environ*, 97, 206–214, <https://doi.org/10.1016/j.atmosenv.2014.08.021>, 2014.

- Arter, C. A. and Arunachalam, S.: Assessing the importance of nonlinearity for aircraft emissions' impact on O₃ and PM_{2.5},
745 *Science of the Total Environment*, 777, 146121, <https://doi.org/10.1016/j.scitotenv.2021.146121>, 2021.
- Atkinson, R.: Gas-phase tropospheric chemistry of volatile organic compounds: 1. Alkanes and alkenes, *J Phys Chem Ref Data*, 26, 215–290, <https://doi.org/10.1063/1.556012>, 1997.
- Bergin, M. S., Russell, A. G., Odman, M. T., Cohan, D. S., and Chameides, W. L.: Single-source impact analysis using three-dimensional air quality models, *J Air Waste Manage Assoc*, 58, 1351–1359, <https://doi.org/10.3155/1047-7503289.58.10.1351>, 2008.
- Blake, D. R. and Rowland, F. S.: Urban leakage of liquefied petroleum gas and its impact on Mexico City air quality, *Science* (1979), 269, 953–956, <https://doi.org/10.1126/science.269.5226.953>, 1995.
- Borge, R., Alexandrov, V., José del Vas, J., Lumbreras, J., and Rodríguez, E.: A comprehensive sensitivity analysis of the WRF model for air quality applications over the Iberian Peninsula, *Atmos Environ*, 42, 8560–8574,
755 <https://doi.org/10.1016/j.atmosenv.2008.08.032>, 2008.
- Carter, W. P. L.: Development of ozone reactivity scales for volatile organic compounds, *J Air Waste Manage Assoc*, 44, 881–899, <https://doi.org/10.1080/1073161x.1994.10467290>, 1994.
- Chang, C. C., Chen, T. Y., Lin, C. Y., Yuan, C. S., and Liu, S. C.: Effects of reactive hydrocarbons on ozone formation in southern Taiwan, *Atmos Environ*, 39, 2867–2878, <https://doi.org/10.1016/j.atmosenv.2004.12.042>, 2005.
- 760 Chang, C. te, Wang, L., Wang, L. J., Liu, C. P., Yang, C. J., Huang, J. C., Wang, C. P., Lin, N. H., and Lin, T. C.: On the seasonality of long-range transport of acidic pollutants in East Asia, *Environmental Research Letters*, 17, <https://doi.org/10.1088/1748-9326/ac8b99>, 2022a.
- Chang, J. H. W., Griffith, S. M., and Lin, N. H.: Impacts of land-surface forcing on local meteorology and ozone concentrations in a heavily industrialized coastal urban area, *Urban Clim*, 45, <https://doi.org/10.1016/j.uclim.2022.101257>,
765 2022b.
- Chen, C. H., Chuang, Y. C., Hsieh, C. C., and Lee, C. S.: VOC characteristics and source apportionment at a PAMS site near an industrial complex in central Taiwan, *Atmos Pollut Res*, 10, 1060–1074, <https://doi.org/10.1016/j.apr.2019.01.014>, 2019.
- Chen, F. and Dudhia, J.: Coupling and advanced land surface-hydrology model with the Penn State-NCAR MM5 modeling system. Part I: Model implementation and sensitivity, *Mon Weather Rev*, 129, 569–585, [https://doi.org/10.1175/1520-0493\(2001\)129<0569:CAALSH>2.0.CO;2](https://doi.org/10.1175/1520-0493(2001)129<0569:CAALSH>2.0.CO;2), 2001.
- 770 Chen, K. S., Ho, Y. T., Lai, C. H., Tsai, Y. A., and Chen, S. J.: Trends in concentration of ground-Level ozone and meteorological conditions during high ozone episodes in the Kao-Ping Airshed, Taiwan, *J Air Waste Manage Assoc*, 54, 36–48, <https://doi.org/10.1080/10473289.2004.10470880>, 2004.
- Chen, P., Zhao, X., Wang, O., Shao, M., Xiao, X., Wang, S., and Wang, Q.: Characteristics of VOCs and their potentials for O₃ and SOA formation in a medium-sized city in Eastern China, *Aerosol Air Qual Res*, 22, 2013–2019, <https://doi.org/10.4209/aaqr.210239>, 2022.

- Chen, S. P., Liu, W. T., Hsieh, H. C., and Wang, J. L.: Taiwan ozone trend in response to reduced domestic precursors and perennial transboundary influence, *Environmental Pollution*, 289, 117883, <https://doi.org/10.1016/j.envpol.2021.117883>, 2021.
- 780 Cheng, F. Y., Jian, S. P., Yang, Z. M., Yen, M. C., and Tsuang, B. J.: Influence of regional climate change on meteorological characteristics and their subsequent effect on ozone dispersion in Taiwan, *Atmos Environ*, 103, 66–81, <https://doi.org/10.1016/j.atmosenv.2014.12.020>, 2015.
- Chi, X., Liu, C., Xie, Z., Fan, G., Wang, Y., He, P., Fan, S., Hong, Q., Wang, Z., Yu, X., Yue, F., Duan, J., Zhang, P., and Liu, J.: Observations of ozone vertical profiles and corresponding precursors in the low troposphere in Beijing, China, 785 *Atmos Res*, 213, 224–235, <https://doi.org/10.1016/j.atmosres.2018.06.012>, 2018.
- Chou, M.-D. and Suarez, M. J.: A shortwave radiation parameterization for atmospheric studies, *NASA Tech*, 15, 1999.
- Chuang, M. T., Chiang, P. C., Chan, C. C., Wang, C. F., Chang, E. E., and Lee, C. Te: The effects of synoptical weather pattern and complex terrain on the formation of aerosol events in the Greater Taipei area, *Science of the Total Environment*, 399, 128–146, <https://doi.org/10.1016/j.scitotenv.2008.01.051>, 2008.
- 790 Cohan, D. S., Hakami, A., Hu, Y., and Russell, A. G.: Nonlinear response of ozone to emissions: Source apportionment and sensitivity analysis, *Environ Sci Technol*, 39, 6739–6748, <https://doi.org/10.1021/es048664m>, 2005.
- Daellenbach, K. R., Stefenelli, G., Bozzetti, C., Vlachou, A., Fermo, P., Gonzalez, R., Piazzalunga, A., Colombi, C., Canonaco, F., Hueglin, C., Kasper-Giebl, A., Jaffrezo, J. L., Bianchi, F., Slowik, J. G., Baltensperger, U., El-Haddad, I., and Prévôt, A. S. H.: Long-term chemical analysis and organic aerosol source apportionment at nine sites in central Europe: 795 Source identification and uncertainty assessment, *Atmos Chem Phys*, 17, 13265–13282, <https://doi.org/10.5194/acp-17-13265-2017>, 2017.
- Dai, P., Ge, Y., Lin, Y., Su, S., and Liang, B.: Investigation on characteristics of exhaust and evaporative emissions from passenger cars fueled with gasoline/methanol blends, *Fuel*, 113, 10–16, <https://doi.org/10.1016/j.fuel.2013.05.038>, 2013.
- Dunker, A. M., Yarwood, G., Ortmann, J. P., and Wilson, G. M.: Comparison of source apportionment and source sensitivity 800 of ozone in a three-dimensional air quality model, *Environ Sci Technol*, 36, 2953–2964, <https://doi.org/10.1021/es011418f>, 2002a.
- Dunker, A. M., Yarwood, G., Ortmann, J. P., and Wilson, G. M.: The decoupled direct method for sensitivity analysis in a three-dimensional air quality model - Implementation, accuracy, and efficiency, *Environ Sci Technol*, 36, 2965–2976, <https://doi.org/10.1021/es0112691>, 2002b.
- 805 Dunker, A. M., Koo, B., and Yarwood, G.: Source apportionment of the anthropogenic increment to ozone, formaldehyde, and nitrogen dioxide by the path-integral method in a 3D model, *Environ Sci Technol*, 49, 6751–6759, <https://doi.org/10.1021/acs.est.5b00467>, 2015.
- Fan, M. Y., Zhang, Y. L., Lin, Y. C., Cao, F., Sun, Y., Qiu, Y., Xing, G., Dao, X., and Fu, P.: Specific sources of health risks induced by metallic elements in PM_{2.5} during the wintertime in Beijing, China, *Atmos Environ*, 246, 118112, 810 <https://doi.org/10.1016/j.atmosenv.2020.118112>, 2021.

- Fountoukis, C., Megaritis, A. G., Skyllakou, K., Charalampidis, P. E., Pilinis, C., Denier Van Der Gon, H. A. C., Crippa, M., Canonaco, F., Mohr, C., Prévôt, A. S. H., Allan, J. D., Poulain, L., Petäjä, T., Tiitta, P., Carbone, S., Kiendler-Scharr, A., Nemitz, E., O'Dowd, C., Swietlicki, E., and Pandis, S. N.: Organic aerosol concentration and composition over Europe: Insights from comparison of regional model predictions with aerosol mass spectrometer factor analysis, *Atmos Chem Phys*, 14, 9061–9076, <https://doi.org/10.5194/acp-14-9061-2014>, 2014.
- 815
- Gallus, W. A. and Bresch, J. F.: Comparison of impacts of WRF dynamic core, physics package, and initial conditions on warm season rainfall forecasts, *Mon Weather Rev*, 134, 2632–2641, <https://doi.org/10.1175/MWR3198.1>, 2006.
- Guenther, A., Karl, T., Harley, P., Wiedinmyer, C., Palmer, P. I., and Geron, C.: Estimates of global terrestrial isoprene emissions using MEGAN (Model of Emissions of Gases and Aerosols from Nature), *Atmos Chem Phys*, 6, 3181–3210, <https://doi.org/10.5194/acp-6-3181-2006>, 2006.
- 820
- Hakami, A., Odman, M. T., and Russell, A. G.: Nonlinearity in atmospheric response: A direct sensitivity analysis approach, *Journal of Geophysical Research D: Atmospheres*, 109, 1–12, <https://doi.org/10.1029/2003JD004502>, 2004a.
- Hakami, A., Harley, R. A., Milford, J. B., Odman, M. T., and Russell, A. G.: Regional, three-dimensional assessment of the ozone formation potential of organic compounds, *Atmos Environ*, 38, 121–134, <https://doi.org/10.1016/j.atmosenv.2003.09.049>, 2004b.
- 825
- Hakami, A., Seinfeld, J. H., Chai, T., Tang, Y., Carmichael, G. R., and Sandu, A.: Adjoint sensitivity analysis of ozone nonattainment over the continental United States, *Environ Sci Technol*, 40, 3855–3864, <https://doi.org/10.1021/es052135g>, 2006.
- Hsu, C. H. and Cheng, F. Y.: Synoptic weather patterns and associated air pollution in Taiwan, *Aerosol Air Qual Res*, 19, 1139–1151, <https://doi.org/10.4209/aaqr.2018.09.0348>, 2019.
- 830
- Huang, Y. S. and Hsieh, C. C.: VOC characteristics and sources at nine photochemical assessment monitoring stations in western Taiwan, *Atmos Environ*, 240, 117741, <https://doi.org/10.1016/j.atmosenv.2020.117741>, 2020.
- Ji, X., Xu, K., Liao, D., Chen, G., Liu, T., Hong, Y., Dong, S., Choi, S. D., and Chen, J.: Spatial-temporal Characteristics and Source Apportionment of Ambient VOCs in Southeast Mountain Area of China, *Aerosol Air Qual Res*, 22, 1–15, <https://doi.org/10.4209/aaqr.220016>, 2022.
- 835
- Kopplitz, S., Simon, H., Henderson, B., Liljegren, J., Tonnesen, G., Whitehill, A., and Wells, B.: Changes in ozone chemical sensitivity in the United States from 2007 to 2016, *ACS Environmental Au*, <https://doi.org/10.1021/acsenvironau.1c00029>, 2021.
- Kusaka, H. and Kimura, F.: Coupling a single-layer urban canopy model with a simple atmospheric model: Impact on urban heat island simulation for an idealized case, *Journal of the Meteorological Society of Japan*, 82, 67–80, <https://doi.org/10.2151/jmsj.82.67>, 2004.
- 840
- Kusaka, H., Hiroaki, K., Kikegawa, Y., and Kimura, F.: A simple single-layer urban canopy model for atmospheric models: Comparison with multi-layer and slab models, *Boundary Layer Meteorol*, 101, 329–358, 2001.

- 845 Kwok, R. H. F., Baker, K. R., Napelenok, S. L., and Tonnesen, G. S.: Photochemical grid model implementation and application of VOC, NO_x, and O₃ source apportionment, *Geosci Model Dev*, 8, 99–114, <https://doi.org/10.5194/gmd-8-99-2015>, 2015.
- Laughner, J. and Cohen, R. C.: Direct observation of changing NO_x lifetime in North American cities, *Science* (1979), 366, 723–727, 2019.
- 850 Lee, Y. C., Wenig, M., and Yang, X.: The emergence of urban ozone episodes in autumn and air temperature rise in Hong Kong, *Air Qual Atmos Health*, 2, 111–121, <https://doi.org/10.1007/s11869-009-0038-y>, 2009.
- Lei, W., De Foy, B., Zavala, M., Volkamer, R., and Molina, L. T.: Characterizing ozone production in the Mexico City Metropolitan Area: A case study using a chemical transport model, *Atmos Chem Phys*, 7, 1347–1366, <https://doi.org/10.5194/acp-7-1347-2007>, 2007.
- 855 Li, J., Yu, S., Chen, X., Zhang, Y., Li, M., Li, Z., Song, Z., Liu, W., Li, P., Xie, M., and Xing, J.: Evaluation of the WRF-CMAQ Model Performances on Air Quality in China with the Impacts of the Observation Nudging on Meteorology, *Aerosol Air Qual Res*, 22, <https://doi.org/10.4209/aaqr.220023>, 2022.
- Li, Y., Lau, A. K. H., Fung, J. C. H., Zheng, J., and Liu, S.: Importance of NO_x control for peak ozone reduction in the Pearl River Delta region, *Journal of Geophysical Research Atmospheres*, 118, 9428–9443, <https://doi.org/10.1002/jgrd.50659>, 2013a.
- 860 Li, Y., Lau, A. K. H., Fung, J. C. H., Ma, H., and Tse, Y.: Systematic evaluation of ozone control policies using an Ozone Source Apportionment method, *Atmos Environ*, 76, 136–146, <https://doi.org/10.1016/j.atmosenv.2013.02.033>, 2013b.
- Li, Z., Li, W., Zhou, R., Miao, X., Lu, J., Wang, Z., Yang, Z., and Wu, J.: Process-based VOCs source profiles and contributions to ozone formation in typical organic solvent-used industries in Hangzhou, *Aerosol Air Qual Res*, 21, <https://doi.org/10.4209/aaqr.210008>, 2021.
- 865 Lin, C. Y., Liu, S. C., Chou, C. C. K., Liu, T. H., Lee, C. te, Yuan, C. S., Shiu, C. J., and Young, C. Y.: Long-range transport of Asian dust and air pollutants to Taiwan, *Terrestrial, Atmospheric and Oceanic Sciences*, 15, 759–784, [https://doi.org/10.3319/TAO.2004.15.5.759\(ADSE\)](https://doi.org/10.3319/TAO.2004.15.5.759(ADSE)), 2004.
- 870 Lin, C. Y., Liu, S. C., Chou, C. C. K., Huang, S. J., Liu, C. M., Kuo, C. H., and Young, C. Y.: Long-range transport of aerosols and their impact on the air quality of Taiwan, *Atmos Environ*, 39, 6066–6076, <https://doi.org/10.1016/j.atmosenv.2005.06.046>, 2005.
- Ling, Z. H. and Guo, H.: Contribution of VOC sources to photochemical ozone formation and its control policy implication in Hong Kong, *Environ Sci Policy*, 38, 180–191, <https://doi.org/10.1016/j.envsci.2013.12.004>, 2014.
- 875 Liu, X., Wang, N., Lyu, X., Zeren, Y., Jiang, F., Wang, X., Zou, S., Ling, Z., and Guo, H.: Photochemistry of ozone pollution in autumn in Pearl River Estuary, South China, *Science of the Total Environment*, 754, 141812, <https://doi.org/10.1016/j.scitotenv.2020.141812>, 2021.
- Liu, Y., Shao, M., Fu, L., Lu, S., Zeng, L., and Tang, D.: Source profiles of volatile organic compounds (VOCs) measured in China: Part I, *Atmos Environ*, 42, 6247–6260, <https://doi.org/10.1016/j.atmosenv.2008.01.070>, 2008.

Luecken, D. J., Napelenok, S. L., Strum, M., Scheffe, R., and Phillips, S.: Sensitivity of ambient atmospheric formaldehyde and ozone to precursor species and source types across the United States, *Environ Sci Technol*, 52, 4668–4675, 880 <https://doi.org/10.1021/acs.est.7b05509>, 2018.

Luecken, D. J., Yarwood, G., and Hutzell, W. T.: Multipollutant modeling of ozone, reactive nitrogen and HAPs across the continental US with CMAQ-CB6, *Atmos Environ*, 201, 62–72, <https://doi.org/10.1016/j.hal.2017.06.001.Submit>, 2019.

Mazzuca, G. M., Ren, X., Loughner, C. P., Estes, M., Crawford, J. H., Pickering, K. E., Weinheimer, A. J., and Dickerson, R. R.: Ozone production and its sensitivity to NO_x and VOCs: Results from the DISCOVER-AQ field experiment, Houston 885 2013, *Atmos Chem Phys*, 16, 14463–14474, <https://doi.org/10.5194/acp-16-14463-2016>, 2016.

Mo, Z., Shao, M., Lu, S., Qu, H., Zhou, M., Sun, J., and Gou, B.: Process-specific emission characteristics of volatile organic compounds (VOCs) from petrochemical facilities in the Yangtze River Delta, China, *Science of the Total Environment*, 533, 422–431, <https://doi.org/10.1016/j.scitotenv.2015.06.089>, 2015.

Nogueira, F. G. E., Lopes, J. H., Silva, A. C., Lago, R. M., Fabris, J. D., and Oliveira, L. C. A.: Catalysts based on clay and 890 iron oxide for oxidation of toluene, *Appl Clay Sci*, 51, 385–389, <https://doi.org/10.1016/j.clay.2010.12.007>, 2011.

Pallavi, Sinha, B., and Sinha, V.: Source apportionment of volatile organic compounds in the northwest Indo-Gangetic Plain using a positive matrix factorization model, *Atmos Chem Phys*, 19, 15467–15482, <https://doi.org/10.5194/acp-19-15467-2019>, 2019.

Pinthong, N., Thepanondh, S., and Kondo, A.: Source identification of VOCs and their environmental health risk in a 895 petrochemical industrial area, *Aerosol Air Qual Res*, 22, 1–18, <https://doi.org/10.4209/aaqr.210064>, 2022.

Pleim, J. E.: A combined local and nonlocal closure model for the atmospheric boundary layer. Part I: Model description and testing, *J Appl Meteorol Climatol*, 46, 1383–1395, <https://doi.org/10.1175/JAM2539.1>, 2007.

Rajput, P., Mandaria, A., Kachawa, L., Singh, D. K., Singh, A. K., and Gupta, T.: Chemical characterisation and source apportionment of PM₁ during massive loading at an urban location in Indo-Gangetic Plain: Impact of local sources and long- 900 range transport, *Tellus B Chem Phys Meteorol*, 68, <https://doi.org/10.3402/tellusb.v68.30659>, 2016.

Reff, A., Eberly, S. I., and Bhawe, P. v.: Receptor modeling of ambient particulate matter data using positive matrix factorization: Review of existing methods, *J Air Waste Manage Assoc*, 57, 146–154, <https://doi.org/10.1080/10473289.2007.10465319>, 2007.

Rossabi, S. and Helmig, D.: Changes in atmospheric butanes and pentanes and their isomeric ratios in the Continental United 905 States, *Journal of Geophysical Research: Atmospheres*, 123, 3772–3790, <https://doi.org/10.1002/2017JD027709>, 2018.

Sillman, S.: The relation between ozone, NO_x and hydrocarbons in urban and polluted rural environments, *Atmos Environ*, 33, 1821–1845, [https://doi.org/10.1016/S1474-8177\(02\)80015-8](https://doi.org/10.1016/S1474-8177(02)80015-8), 1999.

Tao, W. K., Simpson, J., Baker, D., Braun, S., Chou, M. D., Ferrier, B., Johnson, D., Khain, A., Lang, S., Lynn, B., Shie, C. L., Starr, D., Sui, C. H., Wang, Y., and Wetzell, P.: Microphysics, radiation and surface processes in the Goddard Cumulus 910 Ensemble (GCE) model, *Meteorology and Atmospheric Physics*, 82, 97–137, <https://doi.org/10.1007/s00703-001-0594-7>, 2003.

- Tsai, D. H., Wang, J. L., Wang, C. H., and Chan, C. C.: A study of ground-level ozone pollution, ozone precursors and subtropical meteorological conditions in central Taiwan, *Journal of Environmental Monitoring*, 10, 109–118, <https://doi.org/10.1039/b714479b>, 2008.
- 915 Wang, X., Li, J., Zhang, Y., Xie, S., and Tang, X.: Ozone source attribution during a severe photochemical smog episode in Beijing, China, *Sci China B Chem*, 52, 1270–1280, <https://doi.org/10.1007/s11426-009-0137-5>, 2009.
- Wang, X., Fu, T. M., Zhang, L., Cao, H., Zhang, Q., Ma, H., Shen, L., Evans, M. J., Ivatt, P. D., Lu, X., Chen, Y., Zhang, L., Feng, X., Yang, X., Zhu, L., and Henze, D. K.: Sensitivities of ozone air pollution in the Beijing-Tianjin-Hebei area to local and upwind precursor emissions using adjoint modeling, *Environ Sci Technol*, 55, 5752–5762, <https://doi.org/10.1021/acs.est.1c00131>, 2021.
- 920 Wu, F., Yu, Y., Sun, J., Zhang, J., Wang, J., Tang, G., and Wang, Y.: Characteristics, source apportionment and reactivity of ambient volatile organic compounds at Dinghu Mountain in Guangdong Province, China, *Science of the Total Environment*, 548–549, 347–359, <https://doi.org/10.1016/j.scitotenv.2015.11.069>, 2016.
- Wu, P. C. and Huang, K. F.: Tracing local sources and long-range transport of PM10 in central Taiwan by using chemical characteristics and Pb isotope ratios, *Sci Rep*, 11, <https://doi.org/10.1038/s41598-021-87051-y>, 2021.
- 925 Xiao, X., Cohan, D. S., Byun, D. W., and Ngan, F.: Highly nonlinear ozone formation in the Houston region and implications for emission controls, *Journal of Geophysical Research Atmospheres*, 115, 1–12, <https://doi.org/10.1029/2010JD014435>, 2010.
- Xing, J., Wang, S. X., Jang, C., Zhu, Y., and Hao, J. M.: Nonlinear response of ozone to precursor emission changes in China: A modeling study using response surface methodology, *Atmos Chem Phys*, 11, 5027–5044, <https://doi.org/10.5194/acp-11-5027-2011>, 2011.
- 930 Yang, Y. J., Wilkinson, J. G., and Russell, A. G.: Fast, direct sensitivity analysis of multidimensional photochemical models, *Environ Sci Technol*, 31, 2859–2868, <https://doi.org/10.1021/es970117w>, 1997.
- Yarwood, G., Whitten, G. Z., and Jung, J.: Development, Evaluation and Testing of Version 6 of the Carbon Bond Chemical Mechanism (CB6), 2010.
- 935 Yen, M.-C. and Chen, T.-C.: Seasonal variation of the rainfall over Taiwan, *International Journal of Climatology*, 20, 803–809, [https://doi.org/10.1016/0032-5910\(72\)80020-2](https://doi.org/10.1016/0032-5910(72)80020-2), 2000.
- Yu, R., Lin, Y., Zou, J., Dan, Y., and Cheng, C.: Review on atmospheric ozone pollution in china: Formation, spatiotemporal distribution, precursors and affecting factors, *Atmosphere (Basel)*, 12, <https://doi.org/10.3390/atmos12121675>, 2021a.
- 940 Yu, S., Su, F., Yin, S., Wang, S., Xu, R., He, B., Fan, X., Yuan, M., and Zhang, R.: Characterization of ambient volatile organic compounds, source apportionment, and the ozone-NO_x-VOC sensitivities in a heavily polluted megacity of central China: Effect of sporting events and the emission reductions, *Atmospheric Chemistry and Physics Discussions*, 1–61, <https://doi.org/10.5194/acp-2021-293>, 2021b.

- Zhang, Y., Wen, X.-Y., Wang, K., Vijayaraghavan, K., and Jacobson, M. Z.: Probing into regional O₃ and particulate matter pollution in the United States: 2. An examination of formation mechanisms through a process analysis technique and sensitivity study, *J Geophys Res*, 114, 1–31, <https://doi.org/10.1029/2009jd011900>, 2009.
- Zhang, Y., Wang, X., Barletta, B., Simpson, I. J., Blake, D. R., Fu, X., Zhang, Z., He, Q., Liu, T., Zhao, X., and Ding, X.: Source attributions of hazardous aromatic hydrocarbons in urban, suburban and rural areas in the Pearl River Delta (PRD) region, *J Hazard Mater*, 250–251, 403–411, <https://doi.org/10.1016/j.jhazmat.2013.02.023>, 2013.
- 945 Zhao, Q., Bi, J., Liu, Q., Ling, Z., Shen, G., Chen, F., Qiao, Y., Li, C., and Ma, Z.: Sources of volatile organic compounds and policy implications for regional ozone pollution control in an urban location of Nanjing, East China, *Atmos Chem Phys*, 20, 3905–3919, <https://doi.org/10.5194/acp-20-3905-2020>, 2020.
- 950 Zheng, J., Zhang, L., Che, W., Zheng, Z., and Yin, S.: A highly resolved temporal and spatial air pollutant emission inventory for the Pearl River Delta region, China and its uncertainty assessment, *Atmos Environ*, 43, 5112–5122, <https://doi.org/10.1016/j.atmosenv.2009.04.060>, 2009.
- 955